

**Synthesis and Characterization of Silica Supported Co/Nb  
Bimetallic Catalyst for the Production of Synthetic Fuel via Fischer-  
Tropsch**

by

Mir Muhammad Sohaib

14683

Supervisor: Dr. M Tazli Azizan

Co-Supervisor: AP. Dr. Noor Asmawati Mohd Zabidi

Dissertation submitted in partial fulfilment of  
the requirements for the  
Bachelor of Engineering (Hons)  
(Chemical Engineering)

SEPTEMBER 2014

Universiti Teknologi PETRONAS

Bandar Seri Iskandar

31750 Tronoh

Perak Darul Ridzuan

# **CERTIFICATION OF APPROVAL**

## **Synthesis and Characterization of Silica Supported Co/Nb Bimetallic Catalyst for the Production of Synthetic Fuel via Fischer-Tropsch**

By

Mir Muhammad Sohaib

14683

A project dissertation submitted to the  
Chemical Engineering Programme  
Universiti Teknologi PETRONAS  
in partial fulfilment of the requirement for the  
BACHELOR OF ENGINEERING (Hons)  
(CHEMICAL)

Approved by,

---

(Dr. M Tazli Azizan)

UNIVERSITI TEKNOLOGI PETRONAS  
TRONOH, PERAK  
September 2014

## **CERTIFICATE OF ORIGINALITY**

This is to certify that I am responsible for the work submitted in this project, that the original work is my own except as specified in the reference and acknowledgments, and that the original work contained herein have not been undertaken or done by unspecified sources or persons.

---

MIR MUHAMMAD SOHAIB

## ABSTRACT

Fischer Tropsch synthesis has received considerable attention as it offers a viable alternative to produce liquid fuels and chemicals from non-petroleum carbon resources such as biomass, coal and natural gas. The objective of this work is to synthesize, characterize and study the performance of supported bimetallic cobalt (Co) and niobium (Nb) catalyst in Fischer Tropsch synthesis. Supported bimetallic Co and Nb catalyst have been formulated using reverse microemulsion method. 5wt% of nano particles metal loadings were deposited on silica ( $\text{SiO}_2$ ) support. The effect of different metal loading composition of Co and Nb (100:0, 95:5, 90:10, 85:15) on the physiochemical properties of the catalyst has been investigated. The physiochemical properties of the catalyst were studied using field emission electron microscopy (FESEM), transmission electron microscopy (TEM), Brunauer–Emmett–Teller (BET) and  $\text{N}_2$  physical adsorption. The FTS performance of the synthesized catalyst was examined in a fixed-bed Microreactor at  $220^\circ\text{C}$ , atmospheric pressure and  $\text{H}_2/\text{CO}$  ratio of 2:1. Results from the  $\text{N}_2$  physical adsorption shows that addition of niobium decreases the pore area and volume. It also changes the textural structure from non porous to porous. FESEM and TEM results have shown that the metal particles are well dispersed on the support. The average particle sized ranges from 10.61 nm - 25.5 nm. Introduction of niobium to the catalyst changes its shape from spherical to hexagonal and forms fringes on the particles. This indicates the crystalline structure of cobalt particles. The FTS results exhibit that the CO conversion increases with the amount of Nb in the catalyst. The highest CO conversion is obtained from Sample D (85Co15Nb) which is 70.07%. Sample B (95Co5Nb) showed the lowest selectivity towards  $\text{CH}_4$  (6.58%) and highest selectivity towards  $\text{C}_{5+}$  hydrocarbons i.e. 8.79%. All the samples catalysts display high olefin productivity, indicating that the catalysts synthesized are more suitable for olefin production.

## ACKNOWLEDGEMENT

First and foremost, thanks to Almighty Allah for providing His blessings and guidance in completing this final year project within the stipulated time. The author would like to express his gratitude towards his supervisor Dr. M Tazli Azizan, Chemical Engineering Department and co-supervisor Dr. Noor Asmawati Mohd Zabidi, Centralized Analytical Laboratory, Universiti Teknologi PETRONAS. Working under their guidance and supervision has been a privilege. The supervision, support and guidance that they have given despite their hectic schedules is indeed very much appreciated.

The author would also like to thank Ms. Sara Faiz Hanna Tasfy, PhD. Research student from Chemical Engineering Department, Universiti Teknologi PETRONAS who helped him throughout the course of study.

Many thanks to Final Year Project Coordinators and others involved for their immense contributions and efforts in providing students with the necessary guidelines.

The author is grateful for the financial support from the Ministry of Education (Higher Education Department) under MyRA Incentive Grant for CO<sub>2</sub> Rich Natural Gas Value Chain Program.

Besides this the author would like to thank his institution; Universiti Teknologi PETRONAS for allowing him to use the laboratory facilities. Lastly, the author would like to thank his family for their unwavering love and support.

# TABLE OF CONTENTS

<b>CERTIFICATION OF APPROVAL</b>	ii
<b>CERTIFICATE OF ORIGINALITY</b>	iii
<b>ABSTRACT</b>	iv
<b>ACKNOWLEDGEMENT</b>	v
<b>CHAPTER 1 INTRODUCTION</b>	1
1.1 Background	1
1.2 Problem Statement	2
1.3 Objectives	3
1.4 Scope of Study	3
<b>CHAPTER 2 LITERATURE REVIEW</b>	4
2.1 Introduction	4
2.2 Development of Fischer Tropsch Technology	5
2.3 Fischer Tropsch Synthesis	6
2.4 Catalysts for Fischer Tropsch Synthesis	10
2.5 Reverse Microemulsion Method	14
<b>CHAPTER 3 METHODOLOGY</b>	16
3.1 Introduction	16
3.2 Gantt Chart / Key Milestone	18
3.3 Equipments and Chemicals	19
3.4 Preparation of Bimetallic Catalyst	20
3.5 Characterization Techniques	26
3.5.1 Field Emission Scanning Electron Microscope	26
3.5.2 Transmission Electron Microscope (TEM)	27
3.5.3 N <sub>2</sub> physical adsorption	28

3.6	Microreactor Study	28
<b>CHAPTER 4</b>	<b>RESULTS AN DISCUSSION</b>	<b>30</b>
4.1	Introduction	30
4.2	Catalyst Formulation	30
4.3	Characterization of Catalyst	31
4.3.1	Physical Properties	31
4.3.1.1	Textural properties	31
4.3.1.2	Catalyst morphology	36
4.4	Fischer Tropsch Performance	45
<b>CHAPTER 5</b>	<b>CONCLUSION AND RECOMMENDATION</b>	<b>48</b>
5.1	Conclusion	48
5.2	Recommendation	49
<b>REFERENCES</b>		
<b>APPENDICES</b>		<b>52</b>
	Appendix I: Calculation	52
	Appendix II: Raw Data for BET	61
	Appendix III: Mapping from EDX	63

## LIST OF FIGURES

<b>Figure 2.1</b>	Transformation of non-petroleum carbon resources into liquid fuels and chemicals via syngas	4
<b>Figure 2.2</b>	Number of published papers related of FTS from 2000-2011	6
<b>Figure 2.3</b>	FTS overall process scheme	7
<b>Figure 2.4</b>	Stepwise Fischer-Tropsch reaction	8
<b>Figure 2.5</b>	Operating modes of Fischer-Tropsch process	12
<b>Figure 2.6</b>	Microscopic structure of a microemulsion at a given concentration	14
<b>Figure 2.7</b>	Reverse microemulsion method for the synthesis of nanoparticles	15
<b>Figure 3.1</b>	Research project activities	16
<b>Figure 3.2</b>	Project flow of the study	17
<b>Figure 3.3</b>	SiO <sub>2</sub> before and after drying	20
<b>Figure 3.4</b>	Synthesis setup for purging microemulsion A with helium	21
<b>Figure 3.5</b>	Before and after the formation of microemulsion mixture	22
<b>Figure 3.6</b>	Before and after addition of hydrazine to the solution	22
<b>Figure 3.7</b>	Before and after addition of THF	23
<b>Figure 3.8</b>	Before and after sedimentation	24
<b>Figure 3.9</b>	Vacuum filtration of the sample	24
<b>Figure 3.10</b>	Before and after drying the catalyst overnight	25
<b>Figure 3.11</b>	Before and after calcination of the catalyst	25
<b>Figure 3.12</b>	FESEM equipment	26
<b>Figure 3.13</b>	TEM equipment	27
<b>Figure 3.14</b>	Adsorption equipment	28
<b>Figure 3.15</b>	Microreactor used for catalyst evaluation	29
<b>Figure 4.1</b>	Desorption pore volume plot by BJH method for sample A	32
<b>Figure 4.2</b>	Desorption pore volume plot by BJH method for sample B	32
<b>Figure 4.3</b>	Desorption pore volume plot by BJH method for sample C	33
<b>Figure 4.4</b>	Desorption pore volume plot by BJH method for sample D	33
<b>Figure 4.5</b>	Isotherm liner plot of sample A	34

<b>Figure 4.6</b>	Isotherm liner plot of sample B	34
<b>Figure 4.7</b>	Isotherm liner plot of sample C	35
<b>Figure 4.8</b>	Isotherm liner plot of sample D	35
<b>Figure 4.9</b>	FESEM micrographs of sample A, B and C at 1 KX magnification	37
<b>Figure 4.10</b>	FESEM micrographs of sample A, B and C at 10 KX magnification	38
<b>Figure 4.11</b>	FESEM micrographs of sample A, B and C at 100 KX magnification	39
<b>Figure 4.12</b>	EDX spectrum of catalyst sample A, B, C and D	41
<b>Figure 4.13</b>	TEM images for catalyst samples A, B, C and D	42
<b>Figure 4.14</b>	TEM image showing shape of cobalt particle after addition of Niobium	42
<b>Figure 4.15</b>	Particle size distribution of sample A	43
<b>Figure 4.16</b>	Particle size distribution of sample B	43
<b>Figure 4.17</b>	Particle size distribution of sample C	44
<b>Figure 4.18</b>	Particle size distribution of sample D	44
<b>Figure 4.19</b>	Percentage of CO conversion with respect to time on stream	45
<b>Figure 4.20</b>	Percentage of CH <sub>4</sub> selectivity at different compositions	46
<b>Figure 4.21</b>	Percentage of C <sub>2</sub> -C <sub>4</sub> selectivity at different compositions	46
<b>Figure 4.22</b>	Percentage of C <sub>5+</sub> selectivity at different compositions	47

## LIST OF TABLES

<b>Table 2.1</b>	Factors influencing catalytic activity and product selectivity in FTS	10
<b>Table 2.2</b>	Costs of active metals used as catalyst in Fischer-Tropsch synthesis	11
<b>Table 2.3</b>	Comparison between Co and Fe catalyst	11
<b>Table 2.4</b>	Summary of cobalt based catalyst in the Fischer-Tropsch synthesis	13
<b>Table 3.1</b>	Project Gantt Chart	18
<b>Table 3.2</b>	List of chemicals and equipments	19
<b>Table 3.3</b>	Composition of bimetallic catalyst	20
<b>Table 3.4</b>	Amount of SiO <sub>2</sub> used for each sample preparation	20
<b>Table 3.5</b>	Amount of Triton and C <sub>6</sub> H <sub>12</sub> used for preparation of microemulsion A	21
<b>Table 3.6</b>	Amount of cobalt nitrate and ammonium niobium oxalate used for the preparation of microemulsion B	21
<b>Table 3.7</b>	Amount of hydrazine added for sample preparation	22
<b>Table 3.8</b>	Amount of silica used for sample preparation	23
<b>Table 3.9</b>	Amount of tetrahydrofuran used for sample preparation	23
<b>Table 3.10</b>	Reaction operating conditions	29
<b>Table 4.1</b>	Catalyst composition	30
<b>Table 4.2</b>	Textural properties of the catalysts	32
<b>Table 4.3</b>	EDX elemental analysis for catalyst samples A, B, C and D	40
<b>Table 4.4</b>	Average particle size of the catalyst	44
<b>Table 4.5</b>	Summary of the catalytic performance of the sample catalysts in FTS	47

## ABBREVIATION AND NOMENCLATURES

FTS	Fischer-Tropsch synthesis
Co	Cobalt
Nb	Niobium
WGS	Water gas shift reaction
BTL	Biomass to liquid
CTL	Coal to liquid
GTL	Gas to liquid
HTFT	High temperature Fischer-Tropsch
LTFT	Low temperature Fischer-Tropsch
ASF	Anderson-Schulz-Flory
BET	Brunauer, Emmett and Teller method
FESEM	Field emission scanning electron microscopy
TPR	Temperature-programmed reduction
GC	Gas chromatography
HC	Hydrocarbon
TOS	Time on stream
THF	Tetrahydrofuran

# CHAPTER 1

## INTRODUCTION

### 1.1 BACKGROUND

The rapid reduction of petroleum reserves has encouraged the interest to find new routes to hydrocarbon feedstock. Discovering an appropriate way to utilize world's abundant hydrocarbon resources other than crude oil has attracted considerable interest in recent years. Biogas, biomass, coal, coal-bed gas and natural gas are all hydrocarbon feedstock which can be converted into liquid fuels. However, direct transformation of these non-petroleum hydrocarbon resources into synthetic fuels is relatively complex. One of the most practical ways of transforming these non-petroleum based hydrocarbon feedstock into synthetic fuels is via the Fischer-Tropsch synthesis (FTS). This process was first reported by Franz Fischer and Hans Tropsch in 1923. Liquid fuels derived from the FTS are of high quality and do not contain sulphur or aromatics [1].

Generally, there are three main steps of FTS; production of synthetic gas also known as syngas (a mixture of  $\text{CO} + \text{H}_2$ ), liquefaction of syngas and product upgradation. FTS has two inevitable characteristics; the production of a broad range of hydrocarbons with different chain length and functionalities (diesel, gasoline, light olefins and organic oxygenates), and the discharge of a large amount of heat from the highly exothermic synthesis reaction [2].

The catalyst is the key for further improvement in the efficiency of FTS. Development of catalyst with high activity, selectivity and stability are the areas of focus in the field of FTS research. All the elements of group VIII of the periodic

table display considerable activity towards FTS. Among them cobalt and iron are the most preferred catalysts due to their low cost, high selectivity, more stability towards deactivation and low activity towards the water gas shift reaction (WGS). It has been reported that the addition of two active FTS metals result in physiochemical properties which are unique compared to those expected from monometallic FTS catalysts. These metal particles are usually dispersed on a supports ( $\text{Al}_2\text{O}_3$ ,  $\text{SiO}_2$  and  $\text{TiO}_2$ ) which acts as a carrier and may contribute towards the catalytic activity of the catalyst [3].

In this project study of the synthesis of Cobalt (Co) and Niobium (Nb) bimetallic catalysts using the reverse microemulsion method is reported. The effect of incorporating Nb into Co on the physiochemical properties of silica-supported catalysts in terms of degree of reduction, metal particle size, textural properties and their activities and selectivities in the FTS are presented.

## **1.2 PROBLEM STATEMENT**

The rapid growing global fuel demand and depleting crude oil resources has stimulated the need for finding alternative ways for the utilization of non-petroleum carbon resources for the production of liquid fuels and value added chemicals. Although Fisher Tropsch synthesis is a viable alternate process for the production of synthetic fuel but there is a great need for the development of catalysts with the ability to increase the CO conversion, reduce the selectivity of undesired hydrocarbons product ( $\text{CH}_4$ ) and increase the selectivity of desired hydrocarbon product ( $> \text{C}_{5+}$ ).

Bimetallic cobalt catalysts with Nb loadings have been reported to enhance the selectivity of Fischer-Tropsch synthesis towards high molecular weight hydrocarbons. In this study the reverse microemulsion method has been proposed to synthesize bimetallic Co/Nb catalyst. Based on the earlier research studies, this method has produced better results compared to other catalyst preparation methods such as impregnation method in terms of metal dispersion, surface area and particle size.

Therefore, this research is aimed at synthesizing high performance Silica supported Co/Nb bimetallic catalyst via reverse microemulsion method which has high number of active site, easily reducible and well-dispersed metal particles. The properties of bimetallic catalyst with different compositions of Co and Nb will be studied to determine the best composition for Fischer-Tropsch synthesis.

### **1.3 OBJECTIVES**

The objectives of this project are:

- 1) To synthesize well-dispersed bimetallic catalyst containing cobalt-niobium in different compositions on silica support via reverse microemulsion method.
- 2) To characterize and study the properties of the bimetallic catalyst by applying several characterization methods such as Transmission Electron Microscopy (TEM), Field Emission Scanning Electron Microscopy (FESEM) and N<sub>2</sub> physical adsorption.
- 3) To evaluate the performance of the bimetallic catalyst in a Fischer-Tropsch reaction.

### **1.4 SCOPE OF STUDY**

The scopes of study of this project are:

- 1) Setting up a laboratory scale experiment to prepare Co/Nb bimetallic nanocatalyst by reverse microemulsion method on silicon dioxide (SiO<sub>2</sub>) support.
- 2) Studying the effects of different composition of cobalt and niobium.
- 3) Characterization of nanocatalysts using Transmission Electron Microscopy (TEM), Field Emission Scanning Electron Microscopy (FESEM), and N<sub>2</sub> physical adsorption.
- 4) Performance evaluation of these nanocatalysts.

## CHAPTER 2

### LITERATURE REVIEW

#### 2.1 INTRODUCTION

Shortage of petroleum resources coupled with unpredictable price of crude oil has instigated the need for developing synthetic fuels from non-petroleum resources such as coal, natural gas, coal-bed gas, shale gas, biogas and biomass. FTS has received great significance as it offers clean fuel free from sulphur. In FTS syngas which is produced from carbon sources such as biomass, coal and natural gas is converted to liquid fuels and building block chemicals in the presence of a catalyst. Catalysts used in the FTS include cobalt, iron, nickel and ruthenium. Products obtained from FTS include methane ( $\text{CH}_4$ ), olefins ( $\text{C}_2\text{-C}_4$ ), gasoline ( $\text{C}_5\text{-C}_{12}$ ), diesel ( $\text{C}_8\text{-C}_{21}$ ), wax ( $\text{C}_{25+}$ ) and alcohol (methanol, ethanol and other mixed higher alcohols). **Figure 2.1** shows the transformation of non-petroleum carbon resources into liquid fuels and chemicals via syngas [4].

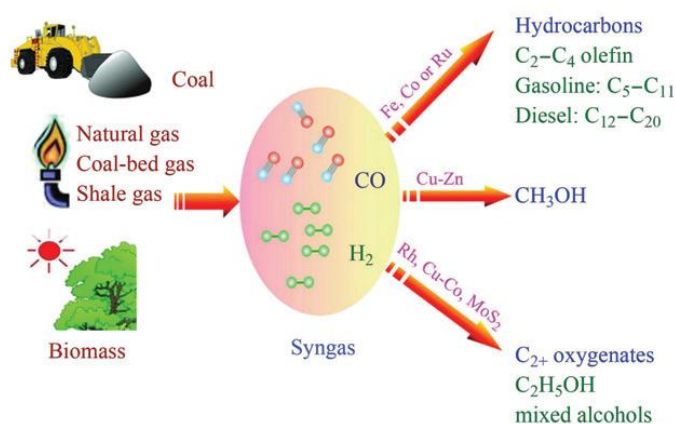


**Figure 2.1:** Transformation of non-petroleum carbon resources into liquid fuels and chemicals via syngas [1]

## 2.2 DEVELOPMENT OF FISCHER-TROPSCH TECHNOLOGY

The development of the FTS started in the beginning of the 20<sup>th</sup> century. During this time Germany faced severe energy crisis due to lack of petroleum reserves. In order to investigate alternates to crude oil for cheap energy and chemical feedstock for industries, Kaiser Wilhelm Institute was constructed. In 1902 Sabatier and Senderens discovered the ability to hydrogenate CO over cobalt and nickel catalysts to convert it to methane. In 1913, BASF recognized the potential of producing hydrocarbons over Co-based catalyst under severe unrealistic conditions. Finally in 1923, Franz Fischer and Hans Tropsch discovered the synthesis of linear hydrocarbons and paraffin using coal derived gas over Fe-based catalyst. This discovery led to the development of modern Fischer-Tropsch catalysts. By 1938, there were twenty FTS plants worldwide, fifteen in Germany with a capacity of 660x130 ton per year [5], four in Japan and one in Manchuria [2].

At present, two FTS plants are being operated in South Africa by SASOL using coal-derived gas, one each in Malaysia and Qatar operated by Shell and ORYX SASOL respectively both of them using natural gas for producing synthetic fuel. Besides this approximately 8-10 different plants are either in construction or planning phase by companies including Bioliq, EniTechnologic, BP, ExxonMobil, Synfuels China, Yankuang group, Shenghua and Synthroleum in countries such as Australia, Bolivia, Chile, China, Egypt, Germany, Indonesia, Iran, Italy, Nigeria, Russia and USA. [1], [6].

Syngas can be produced from a number of methods such as partial oxidation or steam reforming of natural gas and gasification of coal. These processes are highly expensive due to their endothermic nature. Use of natural gas results in lower carbon dioxide (CO<sub>2</sub>) emission compared to the use of coal. Low cost of coal and natural gas has made FTS competitive with crude oil for the production of fuel. SASOL plants use the gasification of coal as the primary source for syngas production. Syngas produced from gasification of coal forms wax at low temperature Fischer-Tropsch (LTFT) reactions and gasoline at high temperature Fischer-Tropsch (HTFT) reactions. On the other hand Shell uses partial oxidation of methane (CH<sub>4</sub>) to produce syngas at high temperature and pressure [5].

In recent years interest in FTS has increased appreciably among the academic community. Based on ISI Web of Science of Thomas Reuters, the number of publications related to FTS rose from 120 in 2000 to 470 in 2011. **Figure 2.2** depicts graph of the number of published papers related to FT synthesis from 2000-2011 [1].

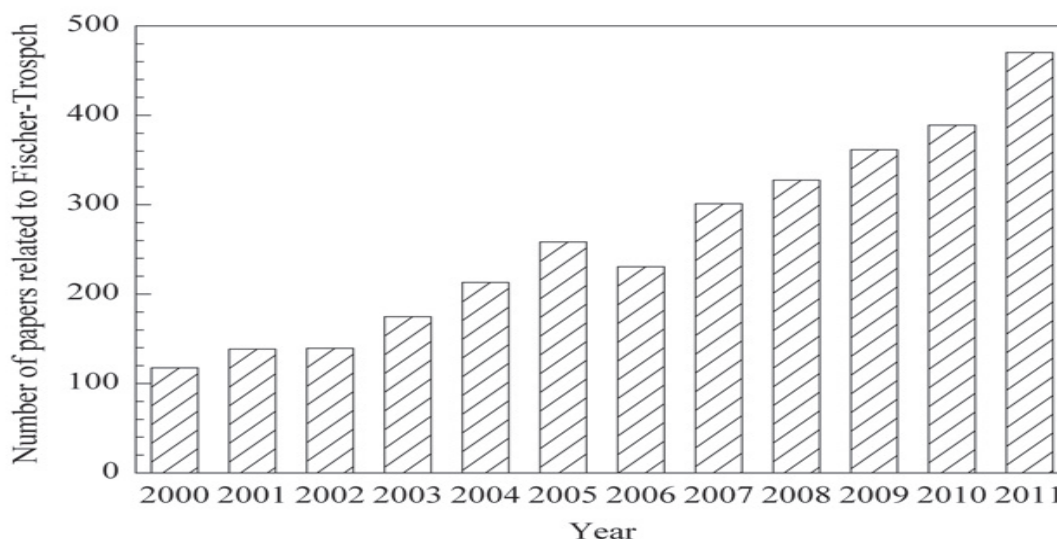
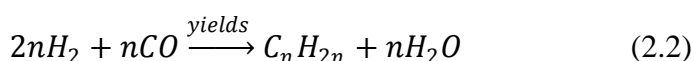
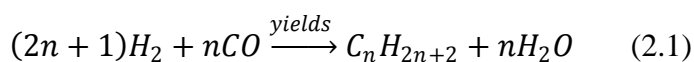


**Figure 2.2:** Number of published papers related of FTS from 2000-2011 [1]

### 2.3 FISCHER-TROPSCH SYNTHESIS

Fischer-Tropsch synthesis has existed as an option for producing synthetic fuel for over 80 years. But it is only recently that it has received more attention due to the dwindling petroleum reserves and environmental constraints. FTS is a process which is aimed at producing synthetic liquid fuels from sources other than crude oil such as biomass, coal and natural gas. FTS involves three main process steps; production of syngas, conversion of syngas to hydrocarbons and product upgrading to produce clean fuels [7]. The chemistry of FTS is an unanticipated phenomenon where the feed gas (mixture of CO and H<sub>2</sub>) is passed over a catalyst inside a reactor to produce liquid hydrocarbons [8]. Reactions taking place during the FTS can be expressed with the equations below [9]:



Products of FTS include methane, diesel, naphtha, gasoline, waxes, oxygenates, etc. The following reactions illustrate the different possibilities of products being formed during FTS (equation 2.3-2.6) [10]:

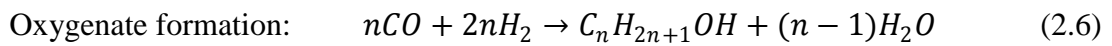
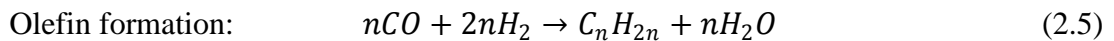
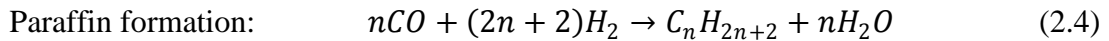
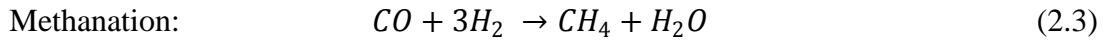


Figure 2.3 shows the overall process configuration of FTS.

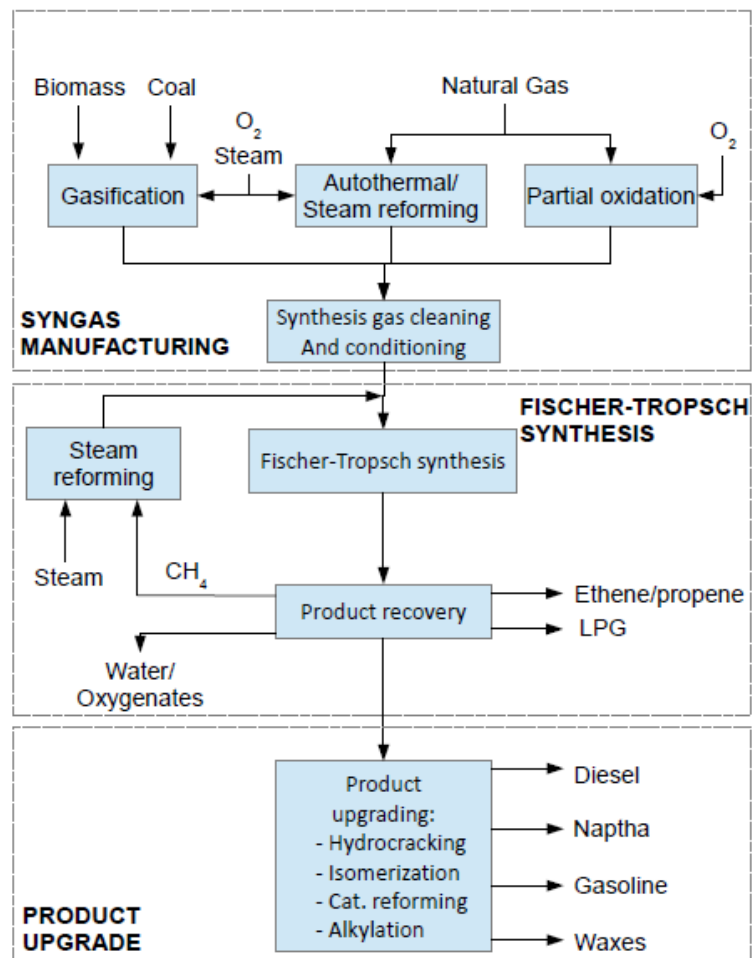
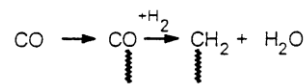


Figure 2.3: FTS overall process scheme

FTS follows the catalytic polymerization reaction where the formation of products is dependent on the chain growth probability. Various factors affecting the length of the chain include the nature of the catalyst, feed gas composition, promoters, pressure and temperature. Fischer-Tropsch reaction passes through three different reaction phases (1) generation of chain initiator due to dissociative chemisorption on the surface of the catalyst, (2) propagation or chain growth due to the coupling of  $\text{CH}_x$  monomers ( $x=0-3$ ) resulting in  $\text{C}_n\text{H}_m$  intermediates and (3) chain termination due to hydrogenation or dehydrogenation of these  $\text{C}_n\text{H}_m$  intermediates. **Figure 2.4** shows the stepwise Fischer-Tropsch reaction [5].

Initiation:



Chain growth and termination:

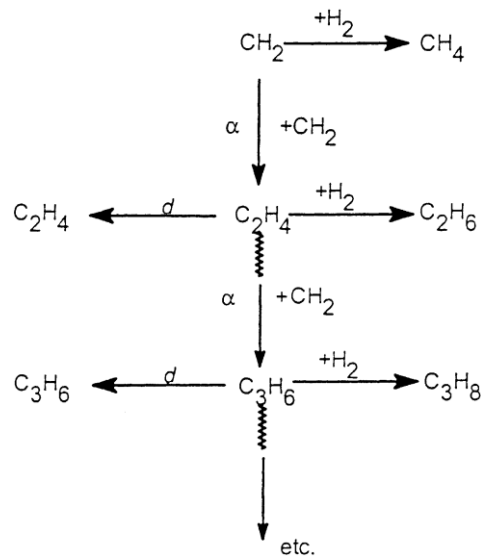


**Figure 2.4:** Stepwise Fischer-Tropsch reaction [5]

Numerous theories have been suggested for Fischer-Tropsch product distribution, one of which is the Anderson-Schulz-Flory (ASF). ASF suggests that the product selectivity is determined by the chain growth probability ( $\alpha$ ), which is a function of the rate of chain growth and termination. Equation 2.7 describes the ASF distribution [11]:

$$M_n = (1 - \alpha)\alpha^{n-1} \quad (2.7)$$

Where,

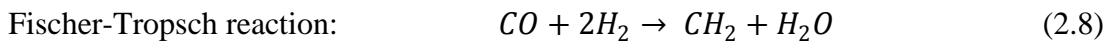
$M_n$ : Molar fraction

$\alpha$ : Chain-growth probability

n: Carbon number

A smaller value of  $\alpha$  leads to lighter hydrocarbons ( $C_1 - C_4$ ) while larger  $\alpha$  value forms heavier ( $C_{21+}$ ) hydrocarbons. The ASF distribution however is unselective for middle-distillate products [1], [11].

FTS is an extremely complex system for producing synthetic fuels but it can be simplified into two main reactions: Fischer-Tropsch (FT) reaction and Water Gas Shift (WGS) reaction. The two reactions are illustrated in equation 2.8 and 2.9 respectively [12].



The two reactions take place simultaneously and are dependent on the catalyst type and gas composition. WGS reaction is controlled by the water availability during the reaction. Most of the water formed will be consumed resulting in the appearance of  $CO_2$  in the product stream. Determination of WGS rate of reaction is extremely important when using syngas with low  $H_2/CO$  ratio as it provides the makeup hydrogen for the FTS [9].

Thus it can be concluded that the performance of FTS depend on several factors, they are [1]:

- (i) Feed gas composition ( $H_2/CO$  ratio)
- (ii) Catalyst type (Ru, Co, Fe)
- (iii) Operating conditions (temperature, pressure)

## 2.4 CATALYSTS FOR FISCHER TROPSCH SYNTHESIS

The key to the chemical transformation is catalysis. It was first introduced in 1836 by Berzelius to explain various decomposition and transformation reactions. Ostwald in 1895, defined the catalyst as species that accelerates chemical reactions without affecting the position of the equilibrium. There are two classification of catalysts; homogenous and heterogeneous. Heterogeneous catalysts are differentiated from homogeneous catalysts by the presence of different phases during reactions. In general, heterogeneous catalysts are preferred over the homogeneous catalysts due to their tolerance of extreme operating conditions and the relative ease of separation from the product stream. Heterogeneous reactions involves numerous steps; adsorption of the reactants onto the solid surface, surface reaction of absorbed species and desorbing of products [9].

The design of a catalyst involves many steps; (1) catalyst synthesis, (2) catalyst activation, (3) catalyst characterization and (4) performance evaluation of catalysts [13]. In FTS, catalyst is the key to further improvement in the efficiency of the process. The focus of research is to develop catalyst with greater stability, higher activity and product selectivity [1]. Various factors that influence the activity and product selectivity of FT catalysts are summarised in **Table 2.1**.

**Table 2.1:** Factors influencing catalytic activity and product selectivity in FTS [1]

<b>Variables influencing activity and product selectivity of a FT catalyst</b>
(i) Reactor design
(ii) Operation conditions
(iii) identity of active metals (Ru, Co or Fe)
(iv) chemical state of active phase (metal, oxide or carbide)
(v) support (identity, pore structure, physiochemical properties)
(vi) promoter
(vii) size of active phase
(viii) microenvironment of active phase

Several elements have been studied as catalysts for FTS. Among them the elements in group VIII of the periodic table display the most considerable activity towards FT reactions [1], [14], [15]. Vannice *et al.* [16] illustrated that the activity of active metals towards the FTS decreased in the sequence as follows:

Ru > Fe > Co > Rh > Ni > Ir > Pt > Pd

The use of ruthenium (Ru) for large-scale industrial purposes is not economically viable as it is a rare metal and is very expensive. Nickel (Ni) is not suitable as it produces a large amount of methane under practical conditions. Therefore, only iron (Fe) and cobalt (Co) based catalysts are applicable for industrial purposes. **Table 2.2** illustrates the relative cost of different active metals used as FT catalysts [5].

**Table 2.2:** Costs of active metals used as catalyst in Fischer-Tropsch synthesis [5]

Approximate relative cost of active metals for Fischer-Tropsch catalysts	
Fe	1
Ni	250
Co	1000
Ru	5000

The first catalysts proposed for the syngas conversion by Franz Fischer and Hans Tropsch were Fe and Co based. Over the years both these metals have been used extensively as FT catalyst in the industry due to their comparatively lower price and higher activity compared to other elements. **Table 2.3** shows a brief comparison between Co and Fe catalysts [14].

**Table 2.3:** Comparison between Co and Fe catalyst [14]

Parameters	Cobalt catalyst	Iron catalyst
Cost	More expensive	Less expensive
Productivity at high conversion	Higher	Lower
Maximal chain growth probability	0.94	0.95
Water gas shift reaction $\text{CO} + \text{H}_2\text{O} \rightarrow \text{CO}_2 + \text{H}_2$	Not very significant; more noticeable at high conversion	Significant
Maximal sulphur content	<0.1 ppm	<0.2 ppm
Required operating pressure	Milder	High
H <sub>2</sub> /CO ratio	~2	~ 0.5 – 2.5

Although Co catalysts are comparatively more expensive than Fe catalysts, but they are more resistant to deactivation. The activity at high conversion is more significant with Co catalysts. WGS reaction with Co catalysts is less significant compared to Fe catalysts. At low temperature Fischer-Tropsch (LTFT) chain growth probabilities of 0.94 and 0.95 have been reported for Co and Fe based catalysts respectively. Both Co and Fe catalyst are sensitive to sulphur contamination. While both Co and Fe catalysts are suitable for LTFT (473 K – 523 K), Co catalysts are not suitable for high temperature Fischer-Tropsch (HTFT) as it leads to significant increase in methane (CH<sub>4</sub>) selectivity. **Figure 2.5** illustrate the two main operating modes of FT processes [9], [14].

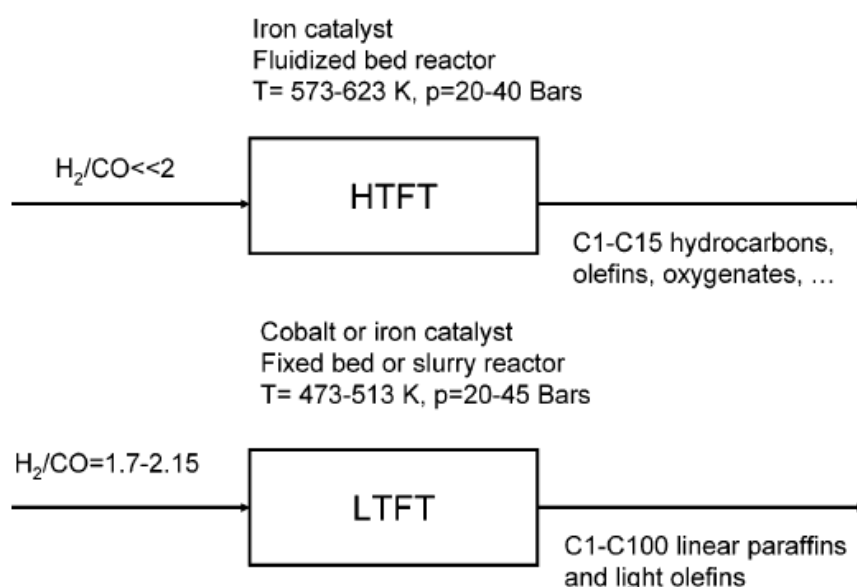


**Figure 2.5:** Operating modes of Fischer-Tropsch process [14]

Because of their high activity, stability and hydrocarbon productivity, Co based catalysts are the optimal choice for the synthesis of synthetic fuels in the LTFT process. The incorporation of second metal component in Co based catalyst enhances the activity and stability compared to its monometallic counterpart. Examples of such bimetallic cobalt catalysts include combinations such as Co-Fe, Co-Mn and Co-Ru. These bimetallic catalysts are dispersed on supports which act as a carrier and contribute to the catalytic activity. Among the most common supports used for bimetallic cobalt catalysts are Al<sub>2</sub>O<sub>3</sub>, SiO<sub>2</sub> and TiO<sub>2</sub> [3],[17]. **Table 2.4** illustrates the summary of different cobalt catalyst used in the FT reaction.

**Table 2.4:** Summary of cobalt based catalyst in the Fischer-Tropsch synthesis

Catalyst	Reaction Conditions	CO conversion (%)	Selectivity (%)	
			CH <sub>4</sub>	C <sub>5+</sub>
Co/Al <sub>2</sub> O <sub>3</sub> [3]	T = 543 K P = 1 bar H <sub>2</sub> /CO = 2	6.3	15.6	3.5
70Co30Fe/Al <sub>2</sub> O <sub>3</sub> [3]	T = 543 K P = 1 bar H <sub>2</sub> /CO = 2	8.1	16.1	3.2
50Co50Fe/Al <sub>2</sub> O <sub>3</sub> [3]	T = 543 K P = 1 bar H <sub>2</sub> /CO = 2	7.5	18.4	2.2
30Co70Fe/Al <sub>2</sub> O <sub>3</sub> [3]	T = 543 K P = 1 bar H <sub>2</sub> /CO = 2	4.2	19.0	1.0
10%Co/Al <sub>2</sub> O <sub>3</sub> [17]	T = 483 K P = 20 bar H <sub>2</sub> /CO = 2	42.6	9.7	80.2
10%Co-0.5%Re/Al <sub>2</sub> O <sub>3</sub> [17]	T = 483 K P = 20 bar H <sub>2</sub> /CO = 2	42.8	8.8	80.8
10%Co/SiO <sub>2</sub> [17]	T = 483 K P = 20 bar H <sub>2</sub> /CO = 2	40.4	9.1	81.7
10%Co-0.5%Re /SiO <sub>2</sub> [17]	T = 483 K P = 20 bar H <sub>2</sub> /CO = 2	40.3	8.7	83.4
10%Co/TiO <sub>2</sub> [17]	T = 483 K P = 20 bar H <sub>2</sub> /CO = 2	39.8	10.2	81.6
10%Co-0.5%Re/TiO <sub>2</sub> [17]	T = 483 K P = 20 bar H <sub>2</sub> /CO = 2	42.6	8.9	84.8
Co/CNT [18]	T = 543 K P = 1 bar H <sub>2</sub> /CO = 2	15.7	17.4	14.0
0.02%Nb/Co/CNT [18]	T = 543 K P = 1 bar H <sub>2</sub> /CO = 2	21.6	12.6	15.1
0.04%Nb/Co/CNT [18]	T = 543 K P = 1 bar H <sub>2</sub> /CO = 2	25.5	7.1	19.5
0.06%Nb/Co/CNT [18]	T = 543 K P = 1 bar H <sub>2</sub> /CO = 2	22.2	7.8	14.3

## 2.5 REVERSE MICROEMULSION METHOD

Oil and water are not miscible in each other and exist in different phases. When they are mixed together both the water and oil phase are saturated with traces of one another. Emulsifier is a substance that is soluble in both solvents and possesses both polar and non polar moieties. In diluted water or oil solution, emulsifier dissolves and is present in homogenous form. Molecules of the emulsifier spontaneously forms aggregates micelles when their concentration exceeds the critical micelle concentration. Mixtures containing water, oil and emulsifier are said to kinetically and thermodynamically stable [19].

A microemulsion is defined as a system of oil, surfactant and water. At macroscopic level, a microemulsion looks like a homogeneous solution but the molecular level the particles are heterogeneous [20]. **Figure 2.6** illustrates different structures of a microemulsion at a given concentration.

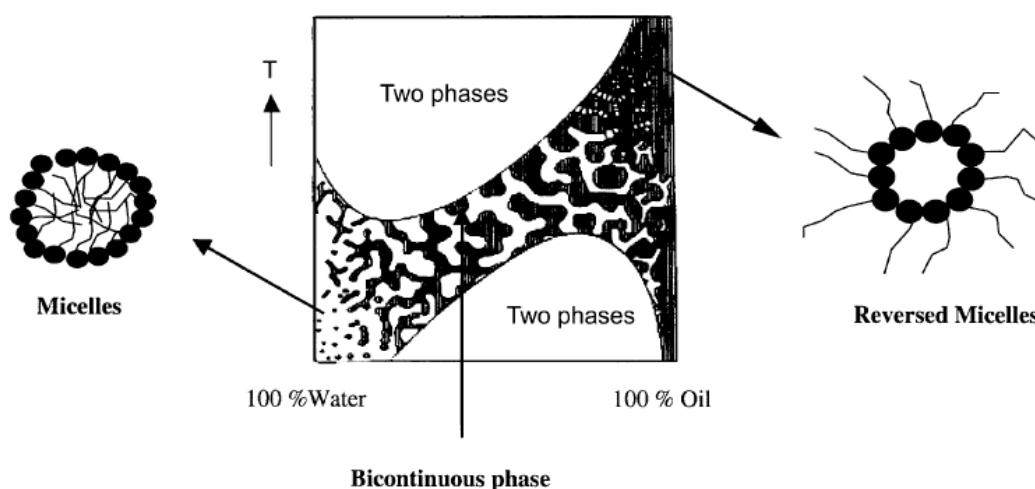


**Figure 2.6:** Microscopic structure of a microemulsion at a given concentration [20]

The properties of nanoparticles prepared using the w/o microemulsion method are influenced by several factors including the nature of precipitating agent, surfactant concentration and size of water droplets. In order to synthesize nanoparticles from the microemulsion method, two microemulsions containing the metal precursor and precipitating agent are mixed together [19]. **Figure 2.7** illustrates the microemulsion method for the synthesis of nanoparticles.

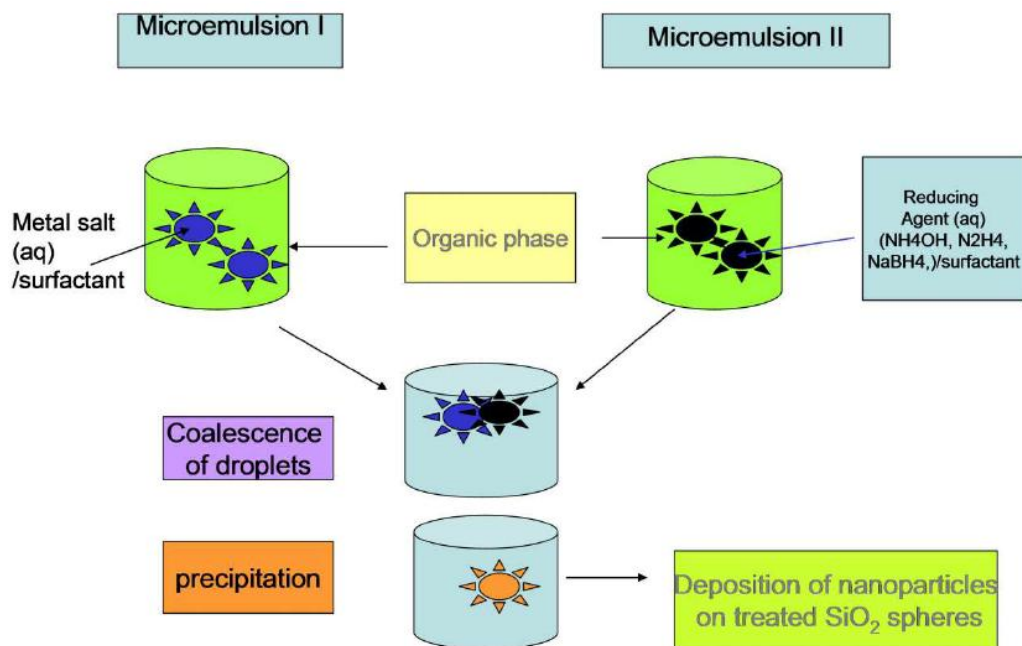


**Figure 2.7:** Reverse microemulsion method for the synthesis of nanoparticles [19]

Reverse microemulsion method has several advantages compared to other methods for catalyst synthesis, they are [21]:

- Thermodynamically stable
- Single optically isotropic
- Spontaneous
- Ultralow interfacial tension of oil and water
- Large interfacial area
- Large capacity to solubilise both aqueous and oil-soluble compounds

## CHAPTER 3

### METHODOLOGY

#### 3.1 INTRODUCTION

Although numerous studies have been conducted on cobalt based catalysts for FTS, further investigation is required to determine the performance of cobalt and niobium bimetallic catalysts. Therefore, this study was aimed to determine the effect of different composition of Co and Nb on the performance of the bimetallic catalyst in FTS. Accordingly, this chapter describes the experimental work conducted in this study. Research project activities of this study were divided into three parts. These are illustrated in **Figure 3.1**.

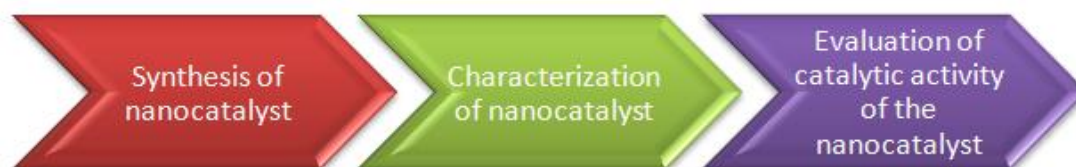


**Figure 3.1:** Research project activities

The first part deals with the synthesis of cobalt and niobium bimetallic catalysts in different compositions supported on SiO<sub>2</sub> support synthesized through the reverse microemulsion method.

In the second part physiochemical properties of the synthesized bimetallic catalysts were determined through several characterization techniques such as FESEM, TEM, and N<sub>2</sub> physical adsorption.

Finally, these catalysts were evaluated in a microreactor system to test their performance in the Fischer-Tropsch reaction. **Figure 3.2** illustrates the project flow for the study.

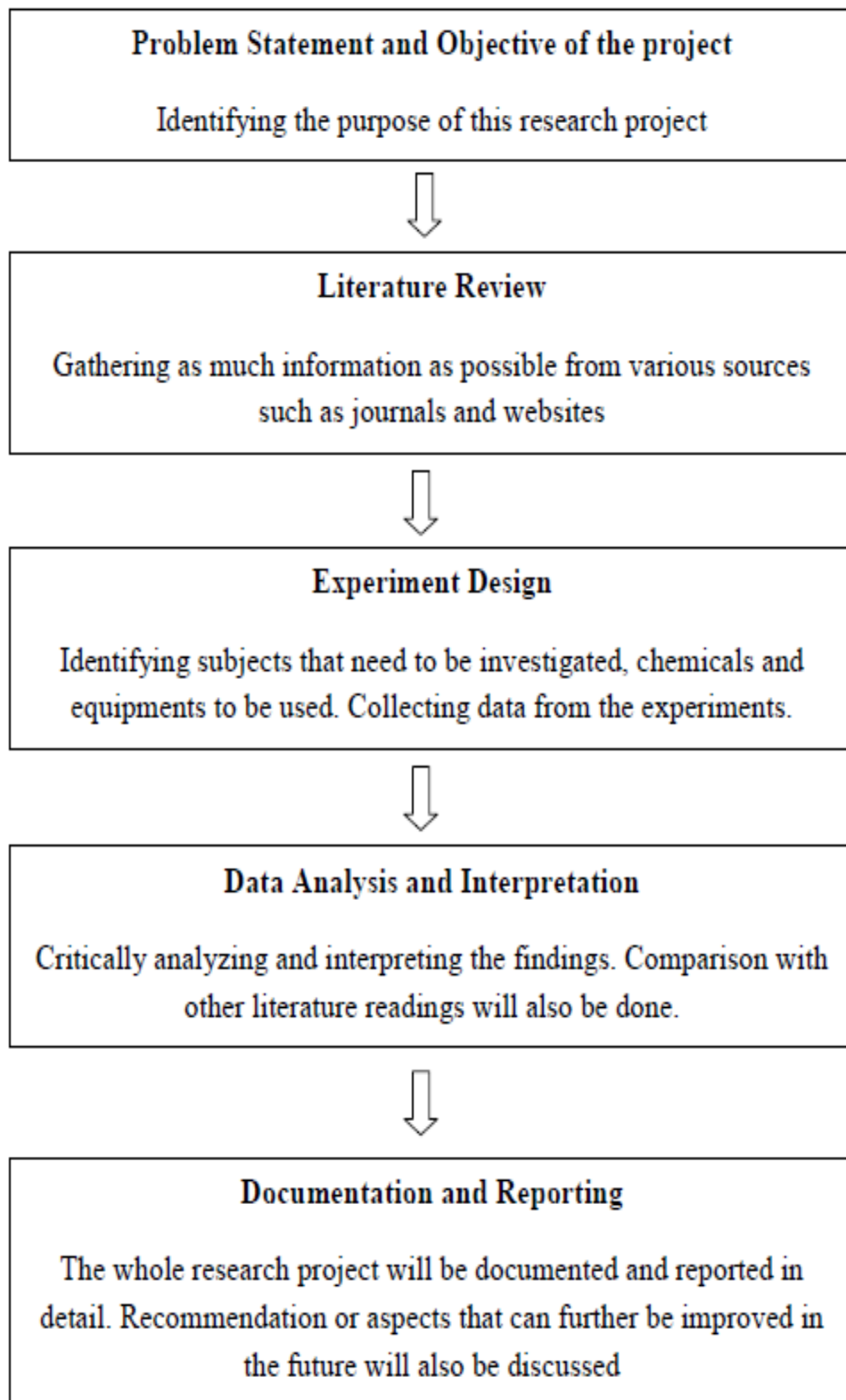


**Figure 3.2:** Project flow of the study

### 3.2 GANTT CHART / KEY MILESTONE

**Table 3.1:** Project Gantt Chart

Activities	FYP 1														FYP 2													
	1	2	3	4	5	6	7	8	9	10	11	12	13	14	1	2	3	4	5	6	7	8	9	10	11	12	13	14
Critical literature review of Fischer-Tropsch reaction, bimetallic nanocatalyst and reverse microemulsion method	█	█	█	█	█	█																						
Requisition of chemicals & laboratory apparatus							█	█	█	█																		
Synthesis of Co/Nb bimetallic nanocatalysts using reverse microemulsion method											█	█	█	█	█	█	█	█										
Characterization of Co/Nb bimetallic nanocatalysts															█	█	█	█	█	█								
Study the activity of catalyst on Fischer-Tropsch reaction																						█	█	█				
Data analysis and interpretation																									█	█	█	█

### 3.3 EQUIPMENTS AND CHEMICALS

**Table 3.2** shows the list of chemicals and equipments used to synthesize and characterize Co/Nb bimetallic catalysts over SiO<sub>2</sub> support.

**Table 3.2:** List of chemicals and equipments

Chemical/Equipments	Supplier/Model	Purity (%)	Quantity	Purpose
Silica Dioxide	Evonik	99.8	11 g	Catalyst Support
Triton X-114	ACROS chemicals	98.0	44.7 g	Surfactant
Cyclohexane (C <sub>6</sub> H <sub>12</sub> )	Aldrich	98.0	400 mL	Surfactant oil phase
Cobalt Nitrate	Merck	99.0	2.8 g	Catalyst Precursor
Ammonium Niobium Oxalate	Aldrich	99.9	0.15 g	Catalyst Precursor
Hydrazine (N <sub>2</sub> H <sub>4</sub> )	Aldrich	98.0	3.2 g	Reducing agent
Tetrahydrofurane	J.T Baker	99.5	1.2 L	Emulsion destabilizing agent
Ethanol	HmbG chemicals	95.0	2 L	Washing
Whatman® Filtration Paper or membrane filter. (For membrane filter, pore size : 0.2 µm Diameter :47 nm)	Whatman®	-	5	Filtrate the solid sample of nanocatalyst
Field Emission Scanning Electron Microscopy (FESEM)	Zeiss Supra 55 VP	-	0.2 g of catalyst for all the tests	Observe morphology of nanocatalyst
Transmission Electron Microscopy (TEM)	Zeiss LIBRA 200 FE	-	0.2 g of catalyst for all the tests	Observe morphology of nanocatalyst (higher resolution)
Stainless Steel Fixed Bed Microreactor	Aseptec Sdn Bhd		0.2 g of catalyst for each reaction	Nanocatalyst catalytic reaction
Volumetric flask 100mL	-	-	1	For Catalyst Preparation
Two-neck round bottom flask	-	-	1	For Catalyst Preparation
Syringe	Terumo	-	5	For adding THF
Syringe pump	Cole Parmer	-	1	For adding THF at a fix flow rate

### 3.4 PREPARATION OF BIMETALLIC CATALYST

Four (4) samples with different composition of Co/Nb were prepared by using cobalt nitrate  $\text{Co}(\text{NO}_3)_2 \cdot 6\text{H}_2\text{O}$  and ammonium niobium oxalate  $\text{C}_4\text{H}_4\text{NNbO}_9 \cdot 6\text{H}_2\text{O}$  on  $\text{SiO}_2$  support. **Table 3.3** illustrates the different composition of cobalt and niobium used for the preparation of the bimetallic catalysts.

**Table 3.3:** Composition of bimetallic catalyst

Sample	Composition of Co:Nb (5 wt%)
A	100:00:00
B	95:05:00
C	90:10:00
D	85:15:00

The procedure for the synthesis of Co/Nb bimetallic catalyst using the reverse microemulsion method is explained below:

- 1)  $\text{SiO}_2$  was dried at  $350^\circ\text{C}$  for three hours. **Table 3.4** shows amount of silica used for each sample. **Figure 3.3** shows the  $\text{SiO}_2$  before and after drying.

**Table 3.4:** Amount of  $\text{SiO}_2$  used for each sample preparation

Sample	Amount of $\text{SiO}_2$ (g)
A	2.75
B	2.75
C	2.75
D	2.75



**Before drying**



**After drying**

**Figure 3.3:**  $\text{SiO}_2$  before and after drying

- 2) Microemulsion A was prepared using Triton X-114 and Cyclohexane ( $C_6H_{12}$ ). First 11.175 g (0.02 mol) of Triton X-114 was poured into 100mL volumetric flask and then it was topped up with Cyclohexane until the 100mL mark was reached. **Table 3.5** shows the amount of Triton and Cyclohexane used for the preparation of each sample.

**Table 3.5:** Amount of Triton and  $C_6H_{12}$  used for preparation of microemulsion A

Sample	Amount of Triton X-114 (g)	Amount of $C_6H_{12}$ (mL)
A	11.175	100
B	11.175	100
C	11.175	100
D	11.175	100

- 3) Microemulsion B was prepared using the catalyst precursor, cobalt nitrate and ammonium niobium oxalate. **Table 3.6** shows the amount of  $Co(NO_3)_2 \cdot 6H_2O$  and  $C_4H_4NNbO_9 \cdot 6H_2O$  used for the preparation of each sample.

**Table 3.6:** Amount of cobalt nitrate and ammonium niobium oxalate used for the preparation of microemulsion B

Sample	Amount of $Co(NO_3)_2 \cdot 6H_2O$ (g)	Amount of $C_4H_4NNbO_9 \cdot 6H_2O$ (g)
A	0.741	0.000
B	0.707	0.023
C	0.667	0.049
D	0.632	0.072

- 4) Microemulsion A was transferred into a two neck round bottom flask and purged with helium gas (He). **Figure 3.4** shows the synthesis setup for purging microemulsion A with helium.



**Figure 3.4:** Synthesis setup for purging microemulsion A with helium

- 5) Microemulsion B was then poured into microemulsion A and stirred vigorously for thirty minutes until microemulsion mixture was formed. **Figure 3.5** shows the mixture of microemulsion A and B.



**After addition of  
microemulsion B to A**

**After formation of  
microemulsion mixture**

**Figure 3.5:** Before and after the formation of microemulsion mixture

- 6) Hydrazine was added to the microemulsion mixture and stirred for five minutes. **Table 3.7** shows the amount of hydrazine added for each sample. **Figure 3.6** shows the solution before and after the addition of hydrazine.

**Table 3.7:** Amount of hydrazine added for sample preparation

Sample	Amount of hydrazine (g)
A	0.814
B	0.793
C	0.788
D	0.782



**Before addition of hydrazine    After addition of hydrazine**

**Figure 3.6:** Before and after addition of hydrazine to the solution

- 7) Silica support was added to the solution and stirred. **Table 3.8** shows the amount of silica used for the preparation of each sample.

**Table 3.8:** Amount of silica used for sample preparation

Sample	Amount of SiO <sub>2</sub> (g)
A	2.85
B	2.85
C	2.85
D	2.85

- 8) Tetrahydrofuran (THF) was then added to the mixture at 1mL/min for 285 minutes. The addition of THF results in fast agglomeration and uncontrolled particle deposition on the support. **Table 3.9** shows the amount of THF added for each sample. **Figure 3.7** shows the solution before and after the addition of THF.

**Table 3.9:** Amount of tetrahydrofuran used for sample preparation

Sample	Amount of THF (g)
A	285
B	285
C	285
D	285

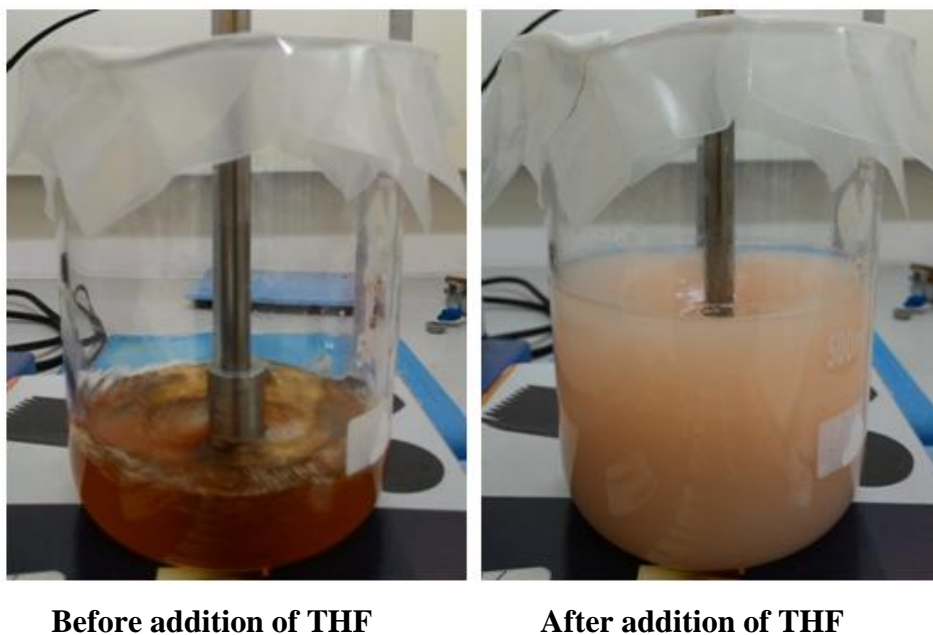


**Figure 3.7:** Before and after addition of THF

- 9) The mixture was left overnight for sedimentation process. The particles slowly sediment down to the bottom of the flask. **Figure 3.8** shows the solution before and after sedimentation.



**Before sedimentation**

**After sedimentation**

**Figure 3.8:** Before and after sedimentation

- 10) The solid catalyst was collected using vacuum filtration and is washed with ethanol several times. **Figure 3.9** shows the vacuum filtration of the sample.

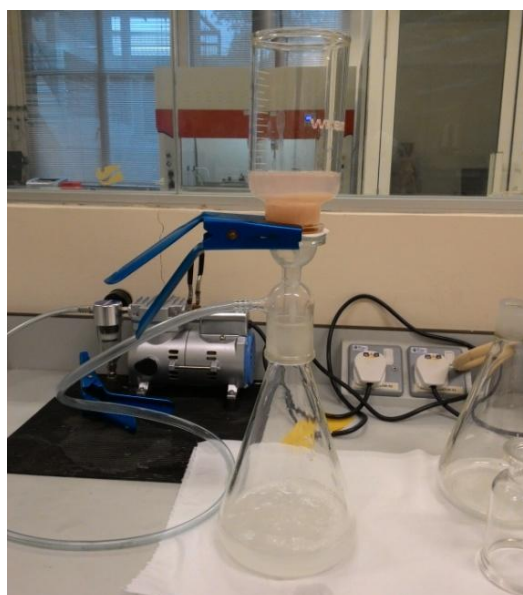
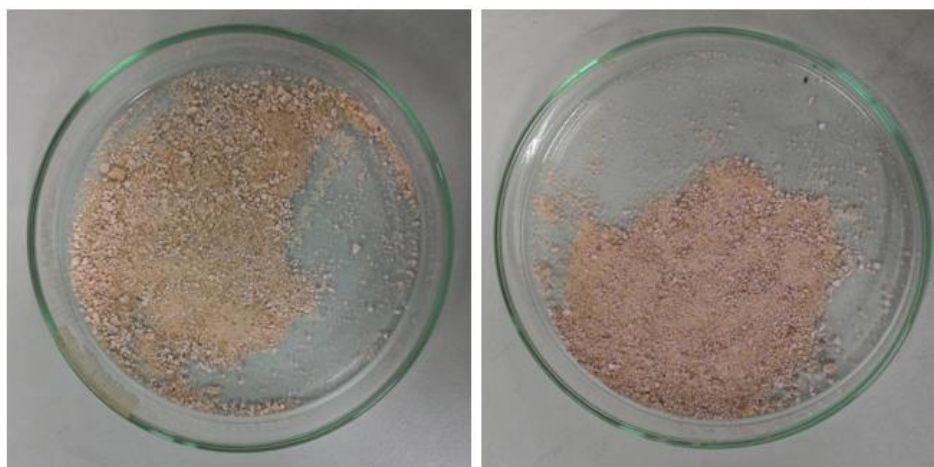


**Figure 3.9:** Vacuum filtration of the sample

11) The catalyst was dried overnight at 120°C. **Figure 3.10** shows the catalyst before and after drying.



**Before drying**

**After drying**

**Figure 3.10:** Before and after drying the catalyst overnight

12) The remaining traces of the surfactant and nitrate precursor were removed by calcining the catalyst under argon flow at 500°C for three hours. The catalyst was then allowed to cool. **Figure 3.11** shows the catalyst before and after calcination.

**Before calcination**



**After calcination**

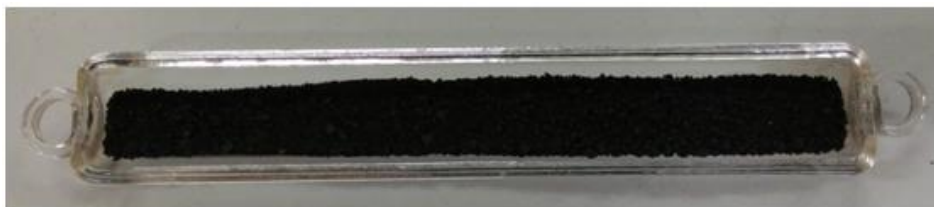


**Figure 3.11:** Before and after calcination of the catalyst

## 3.5 CHARACTERIZATION TECHNIQUES

### 3.5.1 Field Emission Scanning Electron Microscope

Field Emission Scanning Electron Microscope (FESEM) allows the morphological analysis of heterogeneous organic and inorganic material up to nano scale surface structure. FESEM also includes energy dispersive X-ray analysis (EDX), which provides elemental analysis of sample being analyzed.

The FESEM analysis for Co/Nb bimetallic catalyst was performed on Carl Zeiss AG Supra 55 VP equipment. Samples of the catalysts were prepared by sprinkling 0.05 g of the catalyst powder on the carbon tape and shaking off the excess powder.

FESEM was conducted under the following conditions:

Accelerating voltage = 2 KV

Magnification = 1 KX, 10 KX, 100 KX

Working distance = 3.8 – 4.0 mm

**Figure 3.12** shows the FESEM equipment used for the characterization of the catalyst.



**Figure 3.12:** FESEM equipment

### 3.5.2 Transmission Electron Microscope (TEM)

Transmission Electron Microscope was used to analyze the morphology, size, shape and distribution of particles. The TEM analysis for the silica supported Co/Nb bimetallic catalyst was performed on Carl Zeiss AG LIBRA 200 FE. The powdered sample was suspended in iso-propanol and sonicated for 1 hour. A portion of the sample was then deposited on a carbon-coated copper grid. The grid was then placed in the TEM machine to analyze the shape of the nanoparticles, the metal particle size and metal coverage on the support.

TEM was conducted under the following conditions:

Voltage = 200 KV

Magnification = 1000 KX

**Figure 3.13** shows the TEM equipment used for the characterization of the catalyst.



**Figure 3.13:** TEM equipment

### 3.5.3 N<sub>2</sub> physical adsorption

BET theory provides illustrates the relationship between the pressure of gas and the volume of the adsorbed monolayer across the surface of the material. Micromeritics (ASAP 2000) adsorption equipment shown in **Figure 3.14** was used to perform measurements of the total surface area, pore volume and average pore size for all the synthesized silica supported Co/Nb bimetallic catalysts. Samples of the catalysts were prepared by loading 0.3 g of the catalyst onto the pre-weighed quart sample tube



**Figure 3.14:** Adsorption equipment

### 3.6 MICROREACTOR STUDY

The performance of the catalyst in the Fischer-Tropsch process was studied on a fixed-bed reactor supplied by Aseptec Sdn Bhd. The reaction system consisted of three parts namely the gas supply, fixed bed reactor and online gas analysis system. **Figure 3.15** shows the assembly of the microreactor.



**Figure 3.15:** Microreactor used for catalyst evaluation

0.2 g of catalyst was fed into the Microreactor at 1 bar, 220°C and H<sub>2</sub>:CO ratio of 2:1. Prior to the reaction, the catalyst was reduced for four (4) hours at 400°C under 20 mL/min of H<sub>2</sub> flow. The product was analysed via on-line gas chromatograph (GC) to identify the products obtained from the reactor. The reaction conditions used for the samples are given in **Table 3.10**.

**Table 3.10:** Reaction operating conditions

Sample	Mass (g)	Flow rate of CO/H <sub>2</sub> (mL/min)	Reduction Temperature (°C)	Reaction Temperature (°C)	Pressure (bar)	Reaction Time (hrs)
A	0.2	20	400	220	1	5
B	0.2	20	400	220	1	5
C	0.2	20	400	220	1	5
D	0.2	20	400	220	1	5

The output from the GC was used to calculate the percentage of carbon monoxide (CO) and hydrocarbon (HC) conversion using the formulas given below:

$$\text{CO conversion (\%)} = \frac{CO_{in} - CO_{out}}{CO_{in}} \times 100 \quad (3.1)$$

$$\text{CH}_4 \text{ selectivity (\%)} = \frac{\text{Moles of CH}_4}{\text{Total moles of hydrocarbons}} \times 100 \quad (3.2)$$

$$\text{C}_2\text{-C}_4 \text{ selectivity (\%)} = \frac{\text{Moles of C}_2\text{-C}_4}{\text{Total moles of hydrocarbons}} \times 100 \quad (3.3)$$

$$\text{C}_{5+} \text{ selectivity (\%)} = \frac{\text{Moles of C}_{5+}}{\text{Total moles of hydrocarbons}} \times 100 \quad (3.4)$$

$$\text{Olefin Productivity (\%)} = \frac{\text{Moles of Olefin}}{\text{Total moles of hydrocarbons}} \times 100 \quad (3.5)$$

## CHAPTER 4

### RESULTS AND DISCUSSION

#### 4.1 INTRODUCTION

The key to further improve the Fischer Tropsch technology is to develop catalysts high activity, stability and selectivity. This chapter presents the results of the bimetallic catalysts characterization and reaction studies. The results are interpreted in terms of the physical properties and catalytic performance of the catalysts. Physical properties such as morphology, particle size, shape and distribution were determined by FESEM, TEM and N<sub>2</sub> physical adsorption. The effects of different compositions of silica supported Co/Nb bimetallic catalysts in the FTS are discussed in this chapter.

#### 4.2 CATALYST FORMULATION

Four samples of different compositions were prepared based on the calculations shown in APPENDIX 1. **Table 4.1** shows the composition of the four samples.

**Table 4.1:** Catalyst composition

Sample code	Composition
Sample A	100Co/SiO <sub>2</sub>
Sample B	95Co5Nb/SiO <sub>2</sub>
Sample C	90Co10Nb/SiO <sub>2</sub>
Sample D	85Co15Nb/SiO <sub>2</sub>

## 4.3 CHARACTERIZATION OF CATALYST

### 4.3.1 Physical Properties

The physical properties of the bimetallic catalyst include the structural properties, surface morphology and size of metal particles. These were determined through N<sub>2</sub> physical adsorption measurement, FESEM and TEM respectively.

#### 4.3.1.1 Textural properties

The surface area, pore volume, and average pore size of the bimetallic catalysts were measured through N<sub>2</sub> physical adsorption equipment. It is important to measure the surface area and pore volume because any changes to these properties are an indication of pore plugging and material sintering.

The textural properties of the catalysts are shown in **Table 4.2**. The pore volume and average pore size was determined using BJH method as depicted in **Figures 4.1, 4.2, 4.3, 4.4** and their isotherms are shown in **Figures 4.5, 4.6, 4.7 and 4.8**. The raw data for N<sub>2</sub> adsorption studies are shown in Appendix B.

Addition of niobium to the catalyst decreased the pore volume and pore size. The BET surface area was strongly dependent on the ratio of cobalt and niobium. The largest surface area of 4.0061m<sup>2</sup>/g was obtained when the cobalt and niobium ratio was 90:10. Figure 4.2, 4.3 and 4.4 shows that multiple kinds of pores existed in sample B, C and D where as only one kind of pore was obtained from sample A (Figure 4.1). These indicate that the textural properties of catalyst changed from nonporous to porous upon addition of niobium. Sample A follows type III isotherm (Figure 4.5) which indicates weak interaction between adsorbate and adsorbent while sample B,C and D follow type II isotherm (Figure 4.6, 4.7 and 4.8) indicating macroporous adsorbent and unrestricted multilayer adsorption.

**Table 4.2:** Textural properties of the catalysts

Sample	BET Surface Area (m <sup>2</sup> /g)	Pore Volume (cm <sup>3</sup> /g)	Pore Size (nm)
A	2.4135	0.008340	16.35850
B	1.8483	0.003253	11.77000
C	4.0061	0.006123	6.11356
D	3.3366	0.006035	11.23040

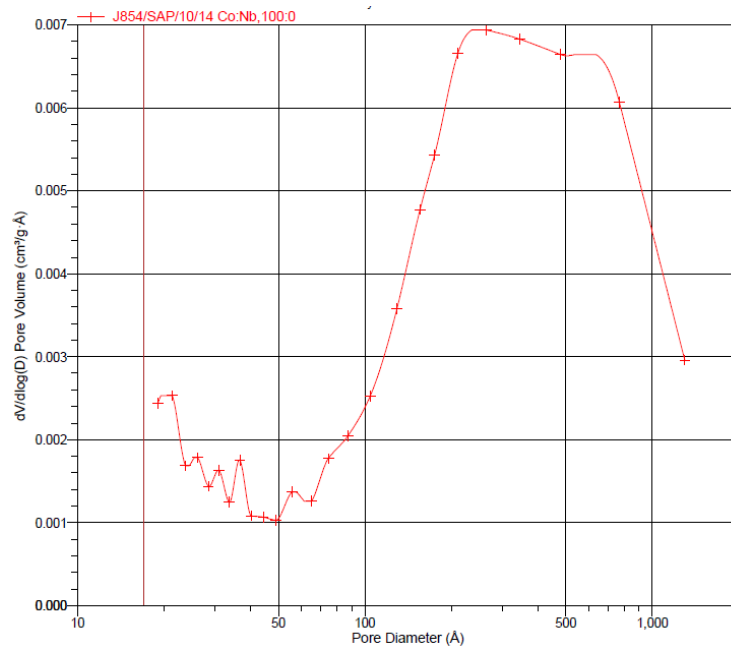


**Figure 4.1:** Desorption pore volume plot by BJH method for sample A

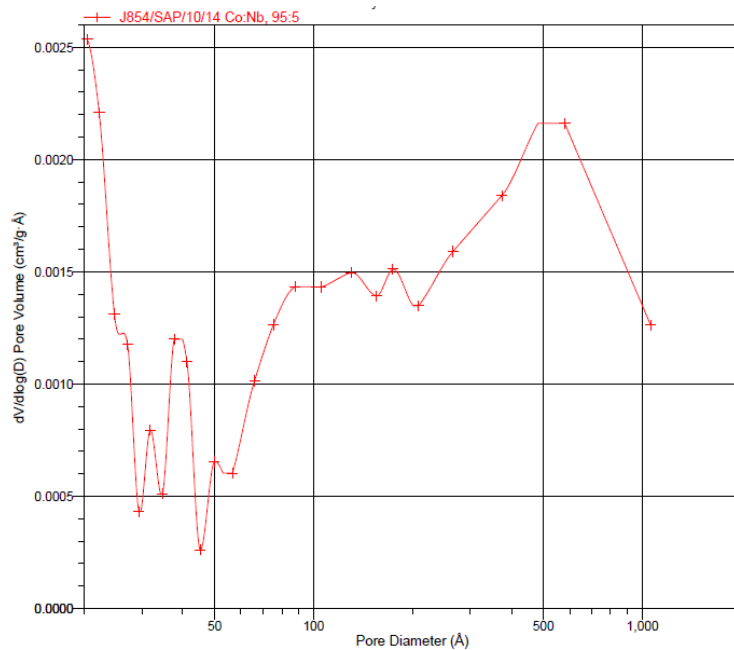


**Figure 4.2:** Desorption pore volume plot by BJH method for sample B

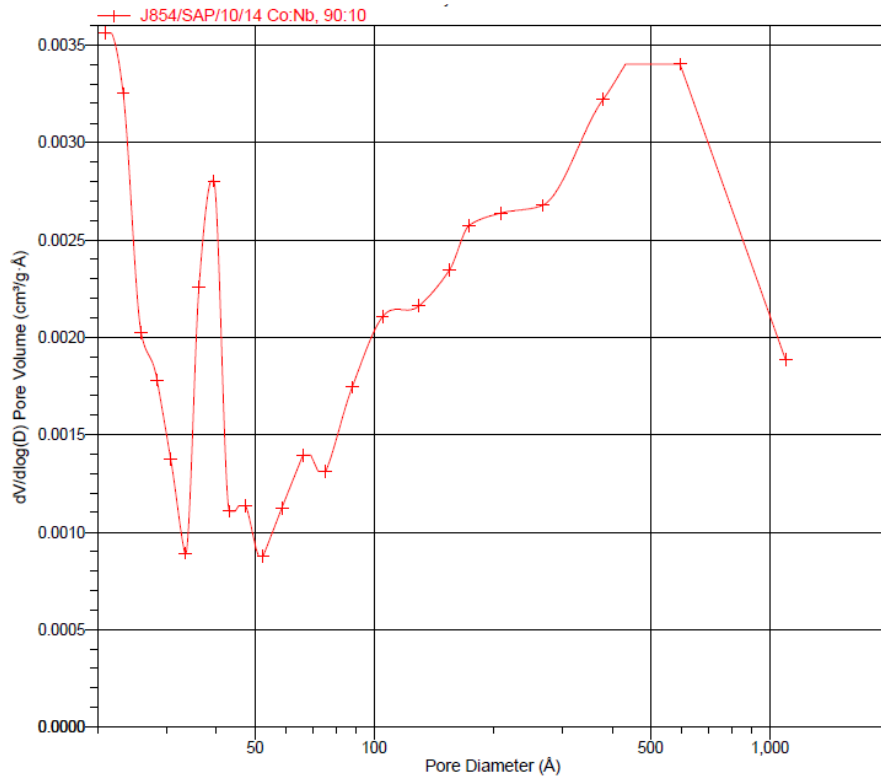


**Figure 4.3:** Desorption pore volume plot by BJH method for sample C

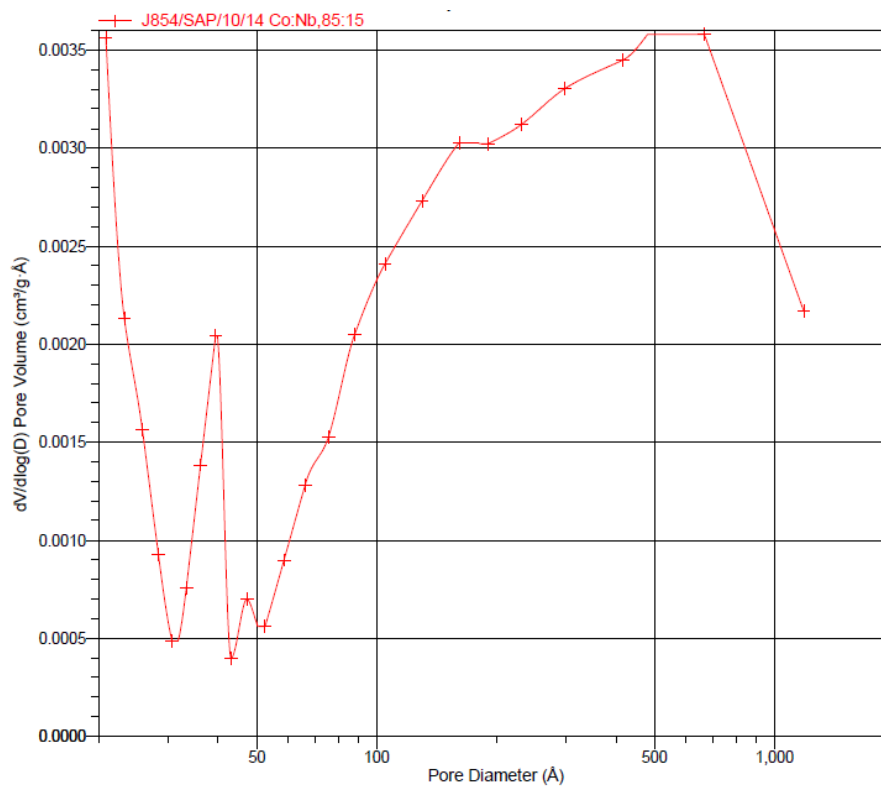


**Figure 4.4:** Desorption pore volume plot by BJH method for sample D

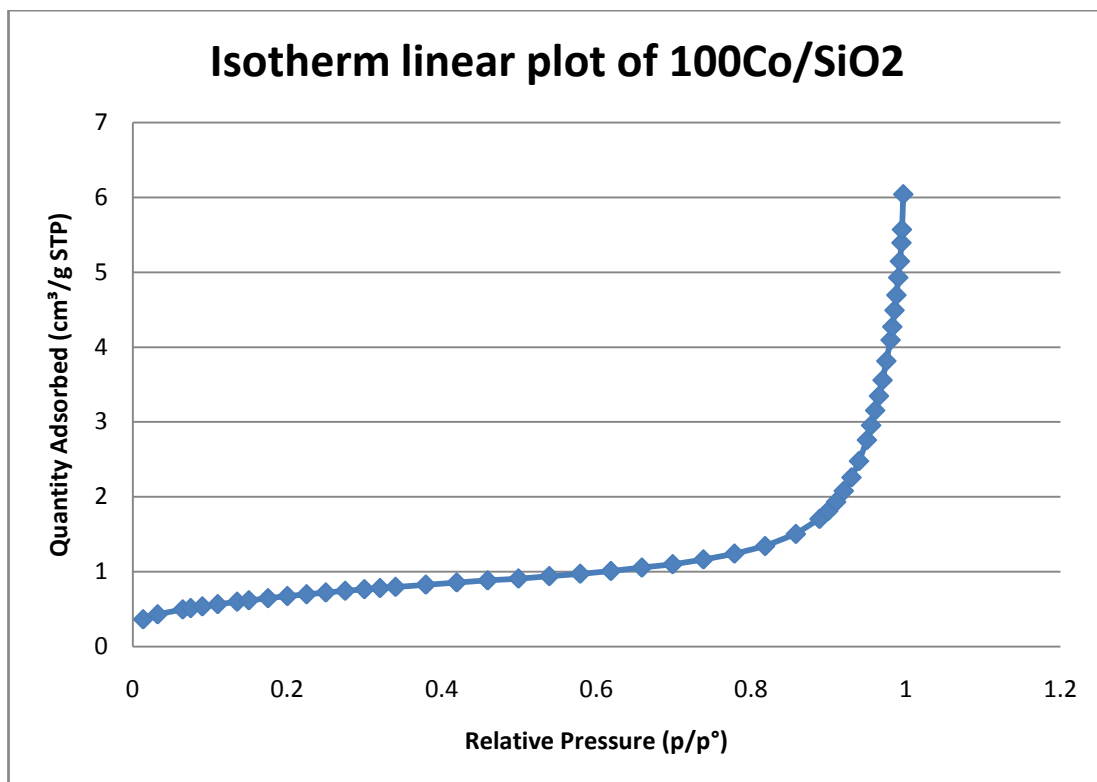


**Figure 4.5:** Isotherm liner plot of sample A

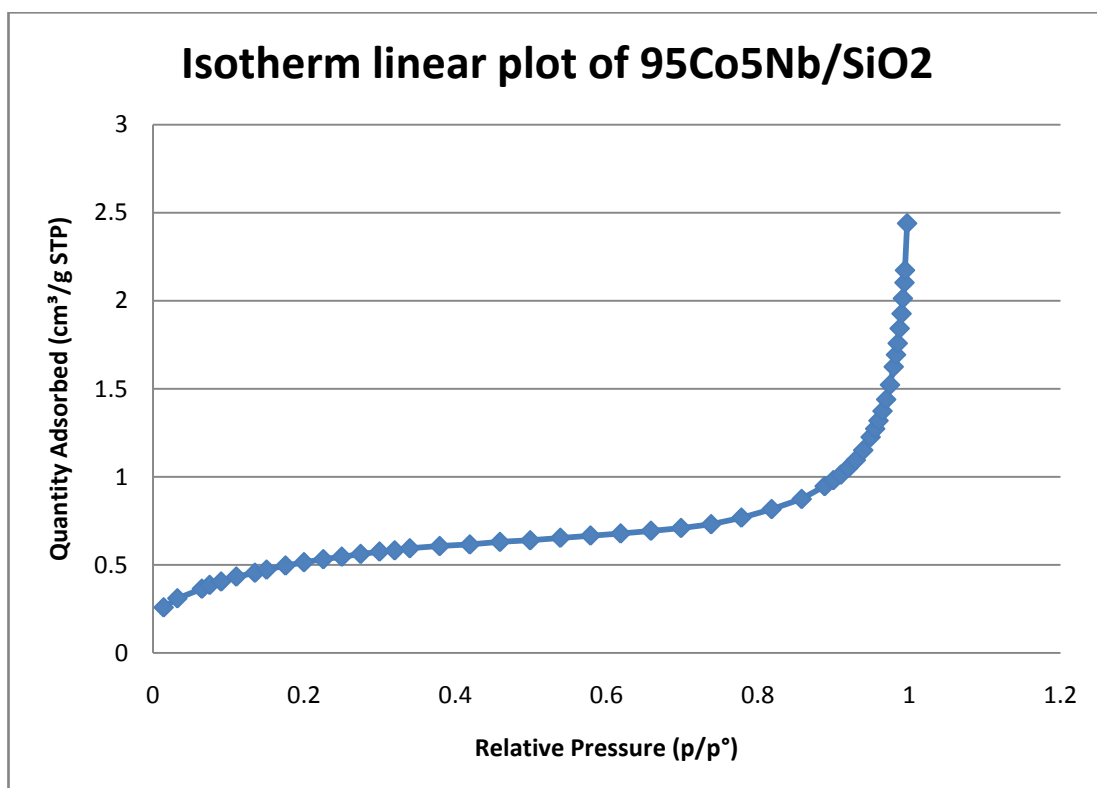


**Figure 4.6:** Isotherm liner plot of sample B

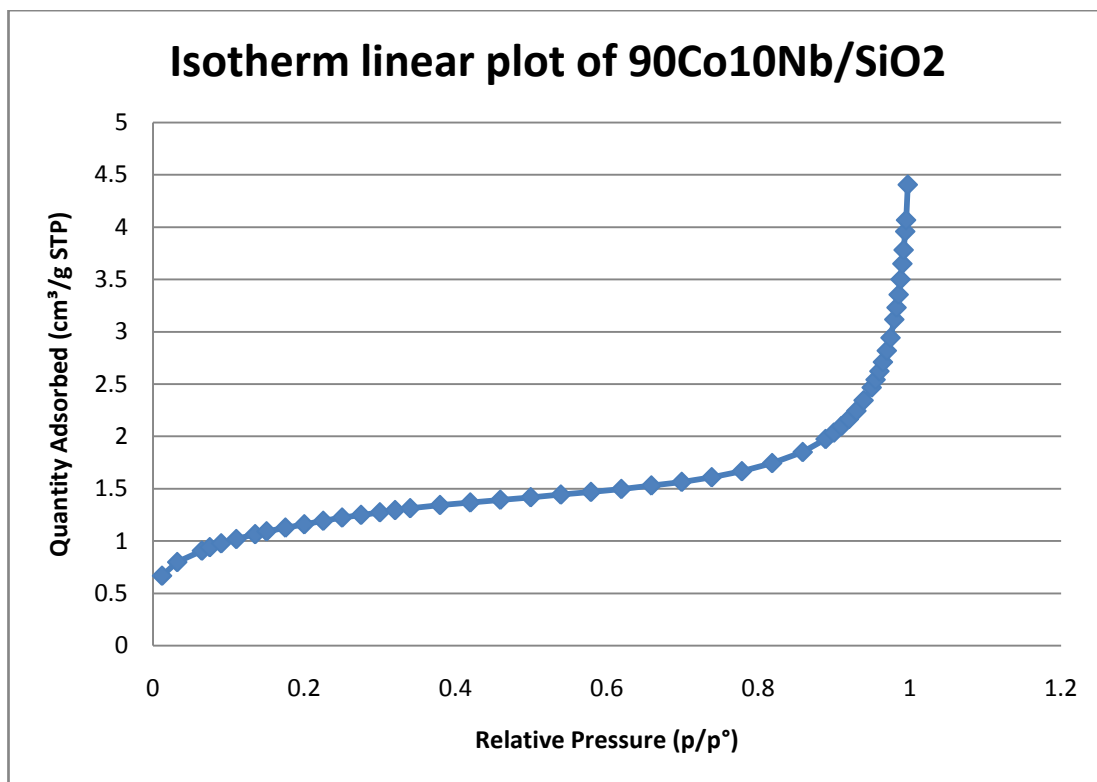


**Figure 4.7:** Isotherm liner plot of sample C

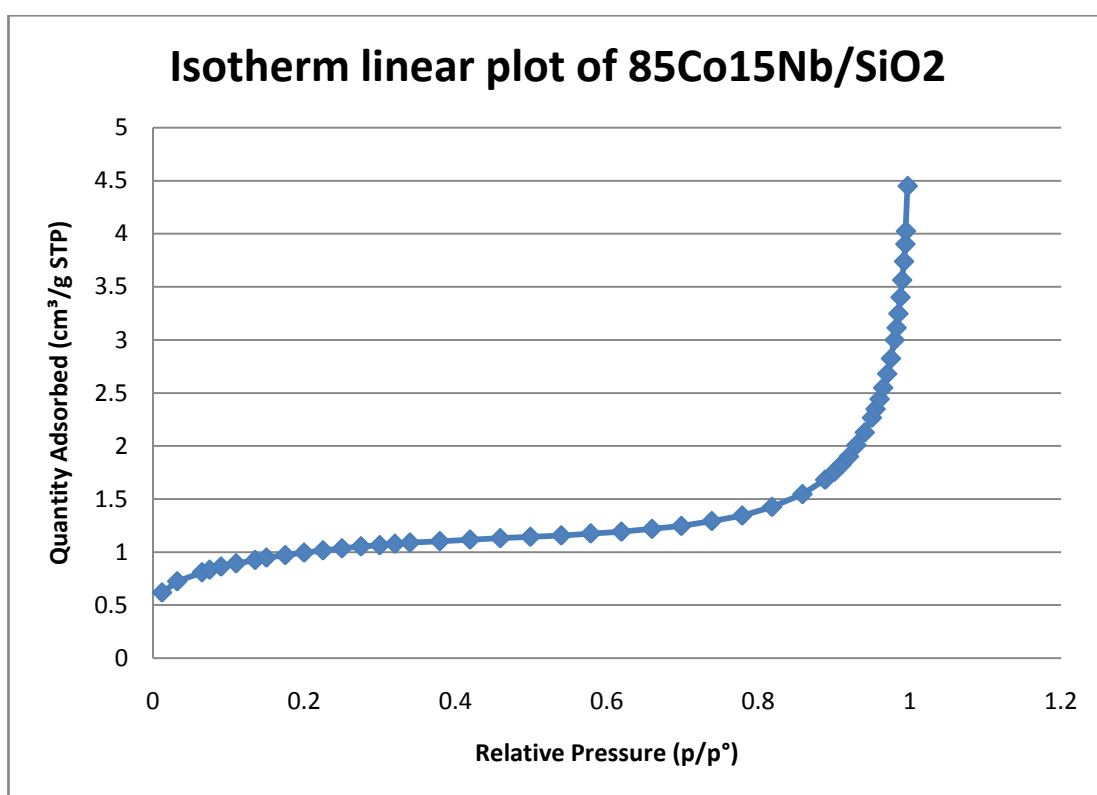


**Figure 4.8:** Isotherm liner plot of sample D

The findings can be summarized as follows:

- Addition of niobium decreased the pore volume and pore size of the catalyst.
- The BET surface area for sample C (90Co10Nb) was the largest among all the catalysts which is  $4.0061\text{m}^2/\text{g}$ .
- Addition of niobium changed textural properties of the catalyst from non porous to porous.
- Sample A follows type III isotherm while sample B, C and D follow type II isotherm.

#### **4.3.1.2 Catalyst morphology**

Field emission electron microscope (FESEM) and transmission electron microscopy (TEM) were used to determine the morphology of the catalyst.

##### **1) Morphology and elemental analysis**

FESEM-EDX analysis was carried out to study the surface properties of silica supported Co/Nb bimetallic catalysts prepared by the reverse microemulsion method.

The morphologies of silica supported Co/Nb bimetallic catalysts at different magnifications are shown in **Figure 4.9, 4.10 and 4.11**. FESEM reveals that the addition of niobium to the catalyst leads to better dispersion of particles and more agglomeration. Sample C shows the most well dispersed particles (Figure 4.9 and 4.10).

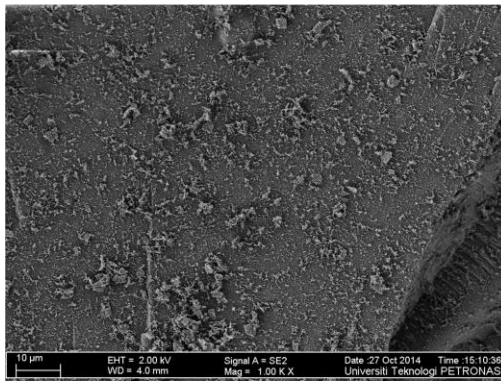
Elemental mapping from EDX was used to determine the distribution of elements and the quantity of elements present in the catalyst. The elemental mapping of the four sample catalysts is shown in Appendix C.



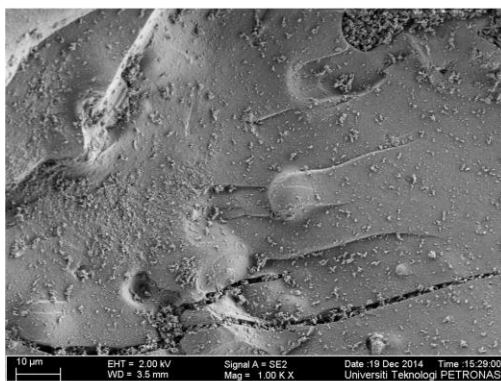
**Sample A**



**Sample B**

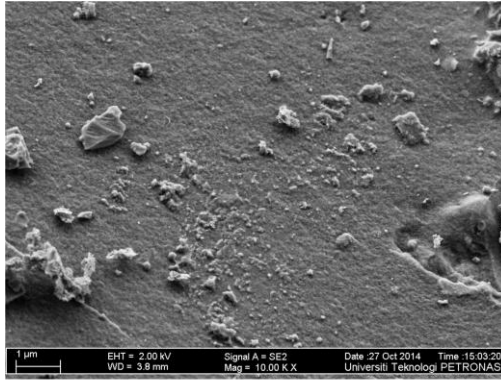


**Sample C**

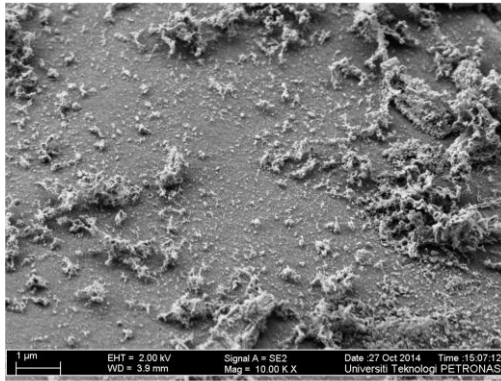


**Sample D**

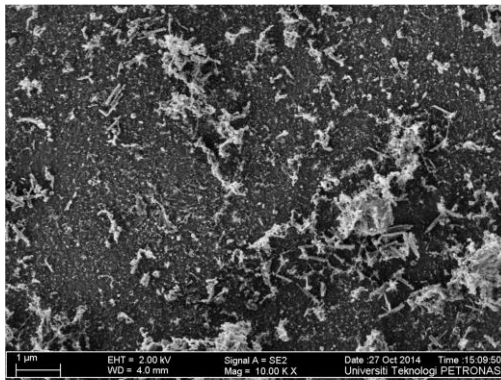
**Figure 4.9:** FESEM micrographs of sample A, B and C at 1 KX magnification



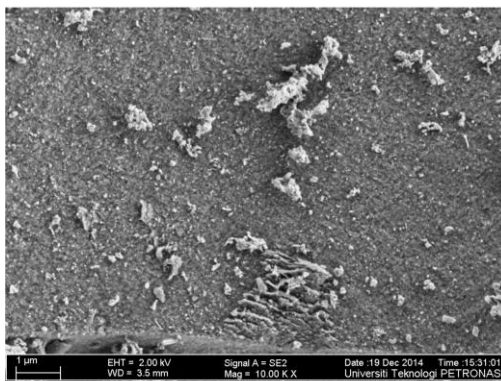
**Sample A**



**Sample B**

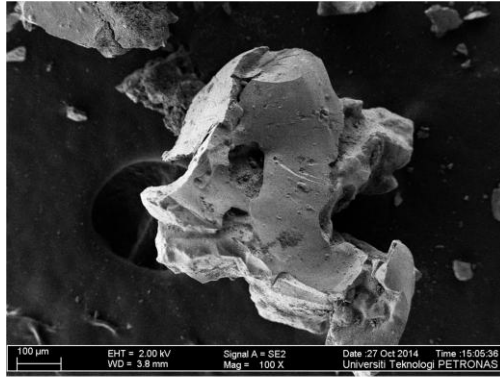


**Sample C**

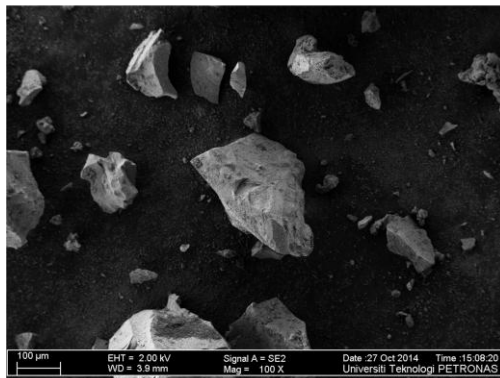


**Sample D**

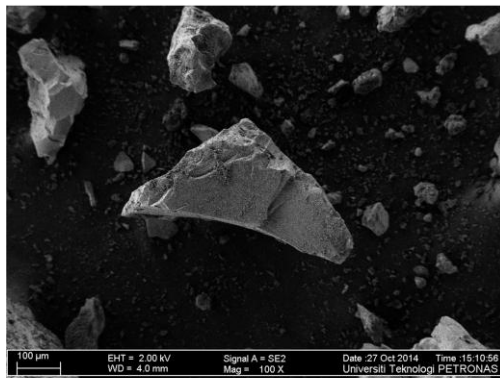
**Figure 4.10:** FESEM micrographs of sample A, B and C at 10 KX magnification



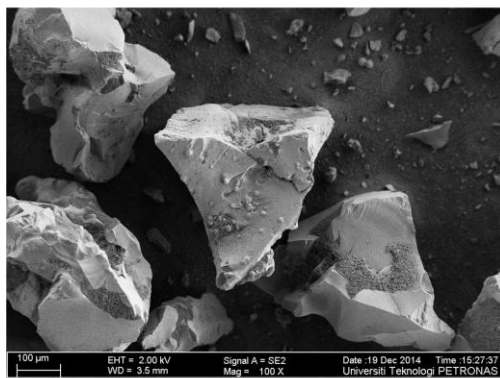
**Sample A**



**Sample B**



**Sample C**



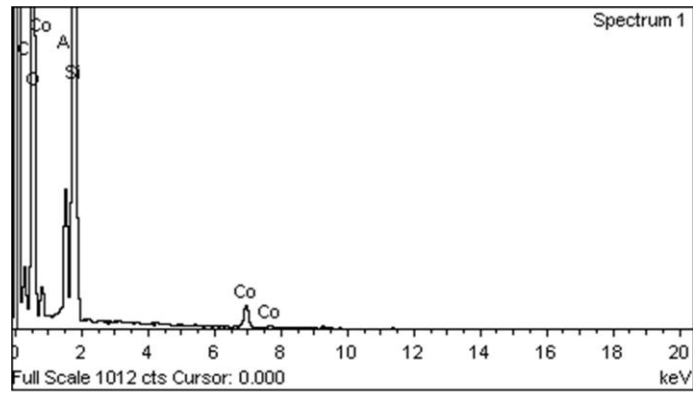
**Sample D**

**Figure 4.11:** FESEM micrographs of sample A, B and C at 100 KX magnification

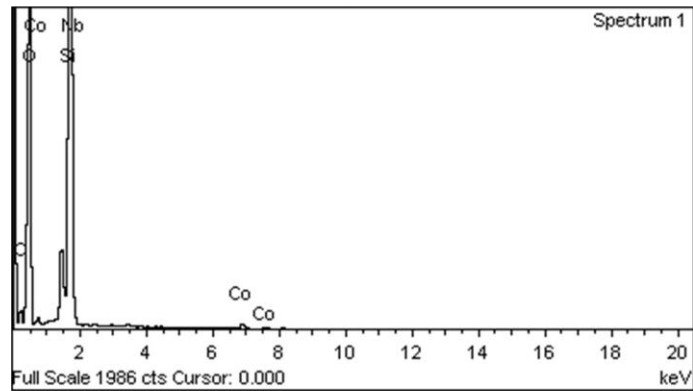
The elemental compositions of the synthesized catalysts were determined using EDX. The results are shown in **Table 4.3** as well as **Figure 4.12**. The values for the elements obtained from the experiment were not in good agreement with the estimated values, which were calculated based on the amount of each element in the catalyst. This deviation can be due to the loss of element during the preparation step or drying and calcination steps.

**Table 4.3:** EDX elemental analysis for catalyst samples A, B, C and D

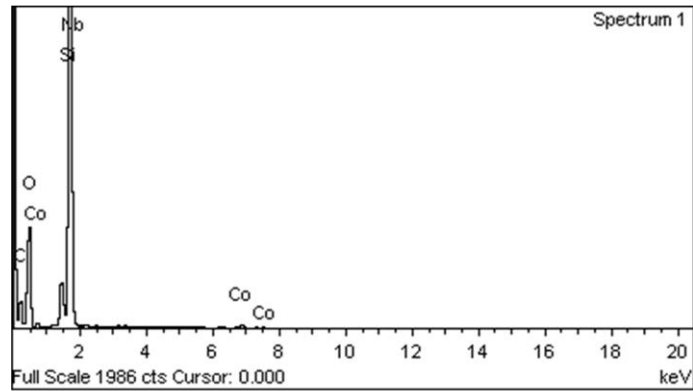
Element	Element composition (wt%)			
	5%Co/SiO <sub>2</sub>	5%Co/Nb/SiO <sub>2</sub>	5%Co/Nb/SiO <sub>2</sub>	5%Co/Nb/SiO <sub>2</sub>
Theoretical value	100%Co	95%Co 5%Nb	90%Co 10%Nb	85%Co 15%Nb
C	21.48	1.99	17.43	13.02
O	51.99	60.86	47.45	45.58
Si	22.06	35.82	33.35	24.46
Co	2.19	1.17	1.37	15.39
Nb	0.00	0.15	0.40	1.26



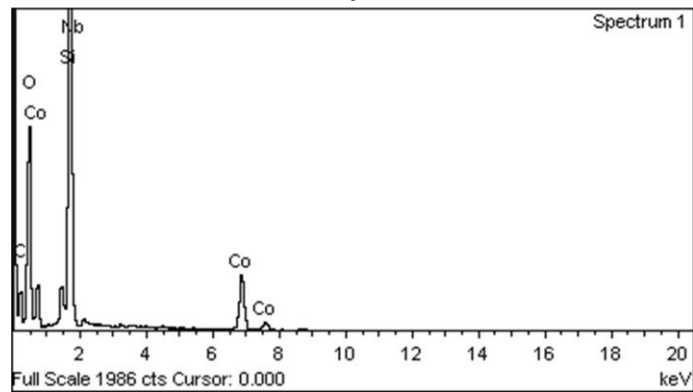
**Sample A**



**Sample B**



**Sample C**



**Sample D**

**Figure 4.12:** EDX spectrum of catalyst sample A, B, C and D

In order better understand the morphology of the silica supported Co/Nb bimetallic catalysts TEM images were studied. **Figure 4.13** shows the TEM images for the catalysts samples A, B, C and D.

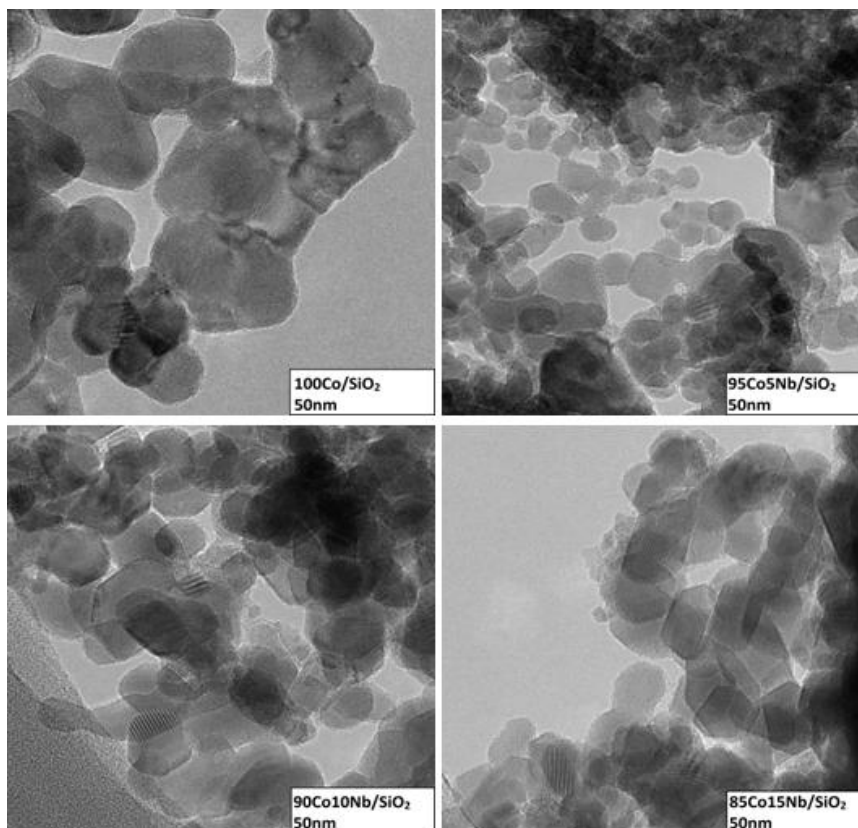


**Figure 4.13:** TEM images for catalyst samples A, B, C and D

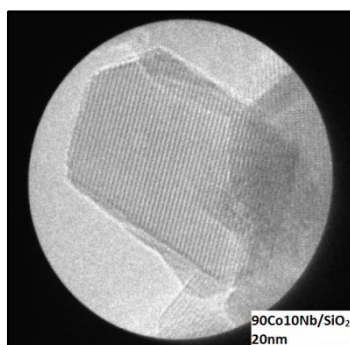


**Figure 4.14:** TEM image showing hexagonal shape of cobalt particle after addition of Niobium

TEM images show that addition of niobium to cobalt changes the shape of particles from spherical to hexagonal in structure (**Figure 4.14**). Particles of sample D which have the highest content of cobalt are perfectly hexagonal in shape. It is also noted

that particles of catalysts with niobium content have fringes indicating crystalline structure.

## 2) Particle size and distribution

TEM technique is used to determine metal particle size and its distribution over the surface of the support. In this study TEM tool was used to measure the particle size of Co crystals and the dispersion of Co particles over SiO<sub>2</sub> support. The average particle size of Co was calculated using 15-20 Co particles over the support. **Figure 4.15, 4.16, 4.17 and 4.18** shows the particle size distribution of sample A, B, C and D respectively. **Table 4.4** shows the average particle size of the bimetallic catalysts.

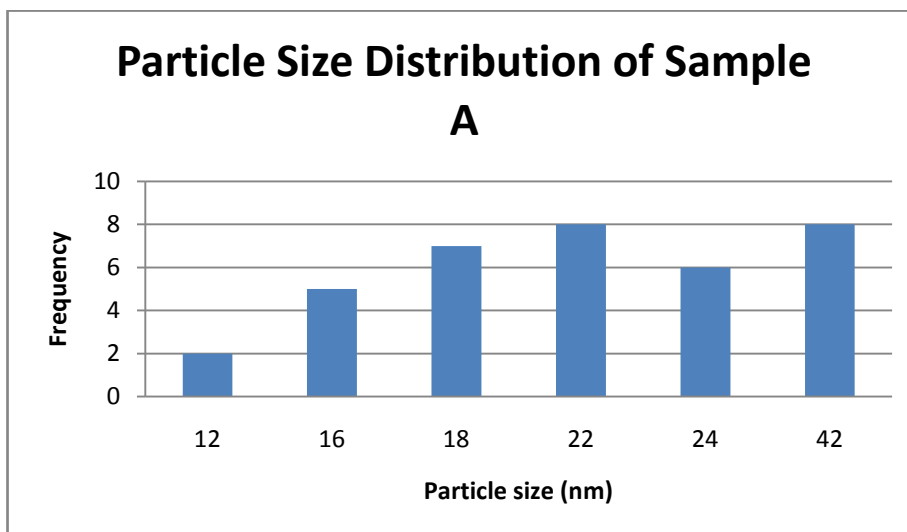


**Figure 4.15:** Particle size distribution of sample A

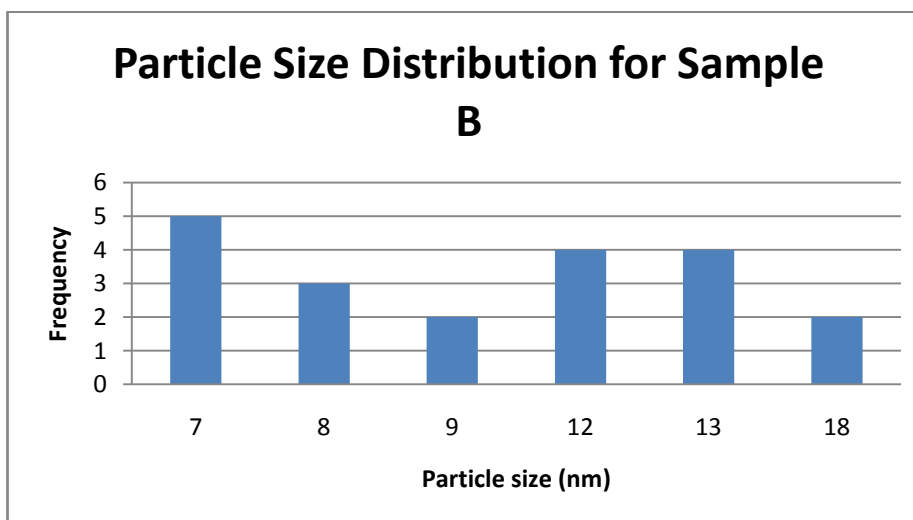


**Figure 4.16:** Particle size distribution of sample B

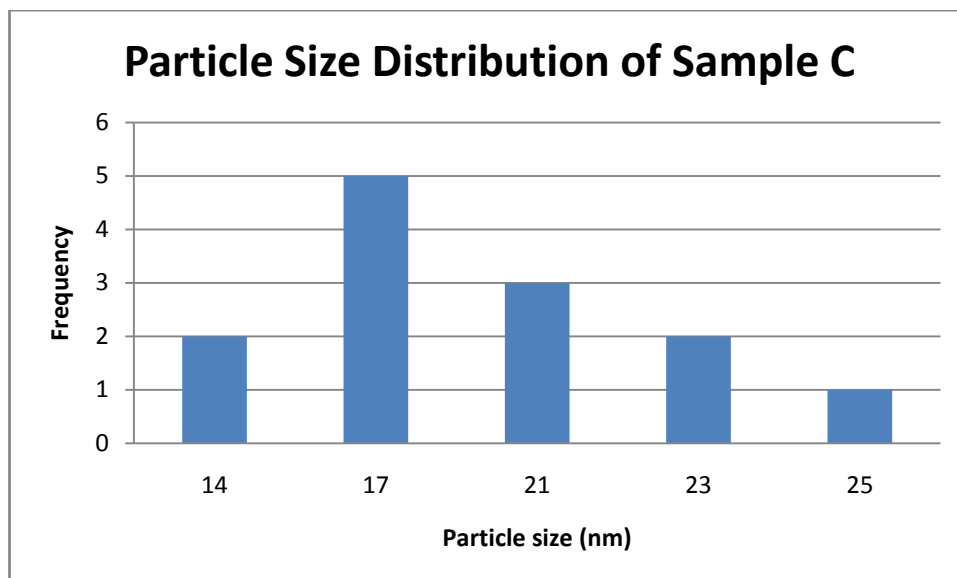


**Figure 4.17:** Particle size distribution of sample C

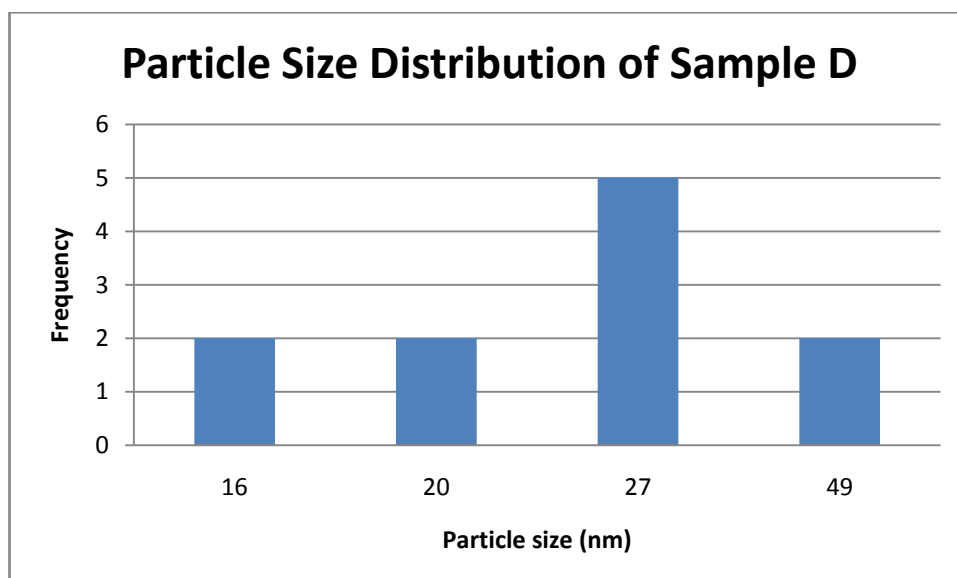


**Figure 4.18:** Particle size distribution of sample D

**Table 4.4:** Average particle size of the catalyst

Sample	Average particle size (nm)
A	24.21±9
B	10.61±3
C	18.85±3
D	25.75±11

All the catalyst samples prepared for this study using the reverse microemulsion method show uniform distribution of particles (**Figure 4.15-4.18**). Sample B had the

smallest particle size and population standard deviation indicating uniform metal distribution over the support.

#### 4.4 FISCHER-TROPSCH PERFORMANCE

The FTS performance of the silica supported Co/Nb bimetallic catalysts were evaluated in a fixed-bed reactor at 220°C and atmospheric pressure. Performance of the catalysts were evaluated in terms of CO conversion and product selectivity.

The stability of the catalyst was represented by the variation of the CO conversion with the time on stream (TOS). The stability of the four sample catalysts are demonstrated in **Figure 4.19**. The CO conversion was found to be time dependent. Compared to Sample D catalyst, all the other catalysts exhibited higher stability. The highest CO conversion was 70.07% exhibited by Sample D where as the lowest was 8.93% exhibited by Sample B.

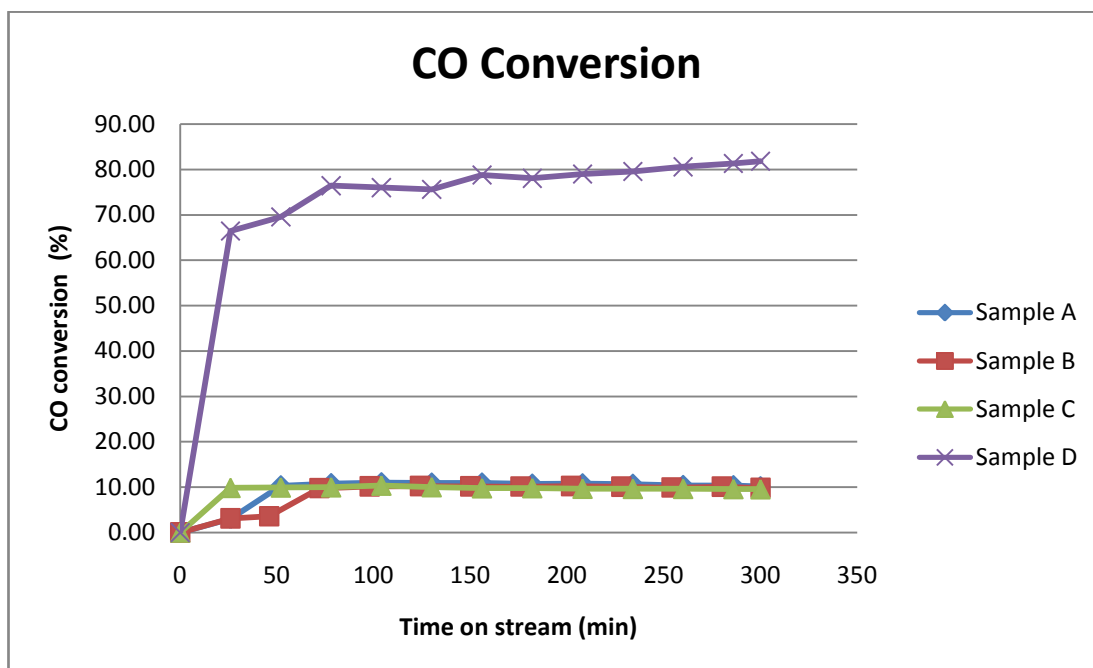


**Figure 4.19:** Percentage of CO conversion with respect to time on stream

**Figure 4.20, 4.21 and 4.22** illustrates the percentage selectivity of the catalysts towards CH<sub>4</sub>, C<sub>2</sub>-C<sub>4</sub> and C<sub>5+</sub> hydrocarbons respectively. **Table 4.5** summarizes the performance of the catalyst in the FTS.

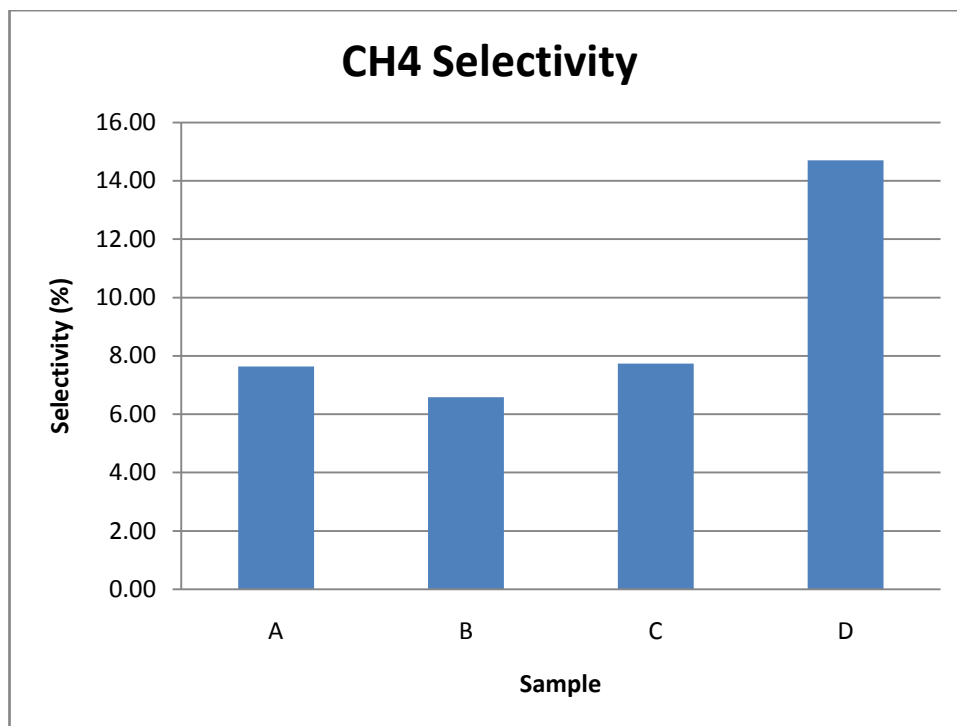


**Figure 4.20:** Percentage of CH<sub>4</sub> selectivity at different compositions

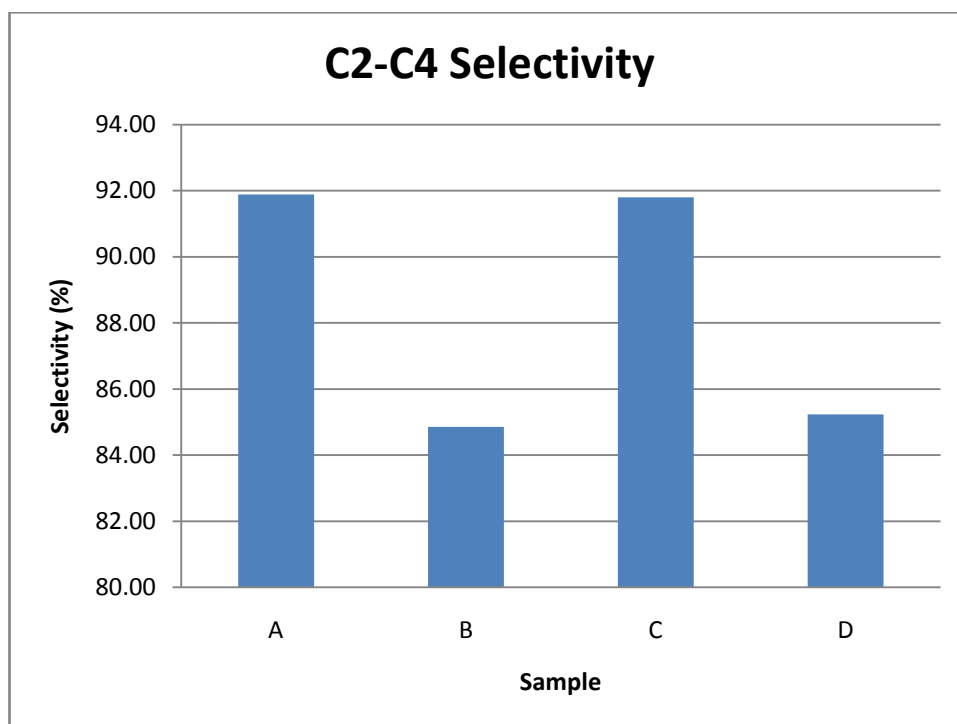


**Figure 4.21:** Percentage of C<sub>2</sub>-C<sub>4</sub> selectivity at different compositions

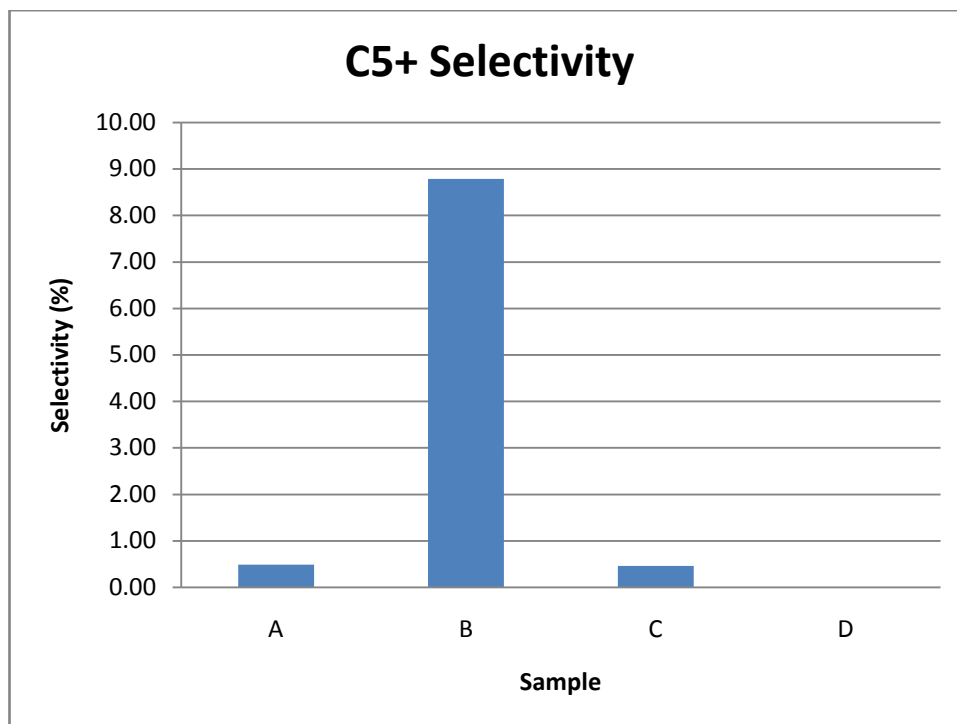


**Figure 4.22:** Percentage of C<sub>5+</sub> selectivity at different compositions

**Table 4.5:** Summary of the catalytic performance of the sample catalysts in FTS

Sample	CO conversion (%)	Selectivity (%)			Olefin Productivity (%)
		CH <sub>4</sub>	C <sub>2</sub> -C <sub>4</sub>	C <sub>5+</sub>	
A	10.00	7.64	91.89	0.49	86.51
B	8.93	6.58	84.85	8.79	86.32
C	9.77	7.74	91.80	0.46	88.74
D	70.07	14.81	85.23	0.06	78.37

In Fischer-Tropsch process it is desired to have low CH<sub>4</sub> selectivity and high C<sub>5+</sub> selectivity. It can be observed from Table 4.5 that the CH<sub>4</sub> selectivity is quite low compared to C<sub>2</sub>-C<sub>4</sub> selectivity. The highest C<sub>5+</sub> selectivity is given by Sample B which is 8.79% while Sample D shows zero selectivity towards C<sub>5+</sub> hydrocarbons. All the prepared sample catalysts display high olefin productivity indicating that they are more suitable for the production of olefin production rather than paraffin productivity.

## CHAPTER 5

### CONCLUSION AND RECOMMENDATION

#### 5.1 CONCLUSION

The objectives of this project have been fully achieved. Four samples of different compositions of cobalt and niobium over silica support have been synthesized using the reverse microemulsion method. The synthesized catalyst have been characterised using several techniques such FESEM, TEM and N<sub>2</sub> physical adsorption. N<sub>2</sub> physical adsorption was done to find the surface area, pore volume and average pore size. It was found that the addition of niobium to the catalyst decreased its pore size and volume. It also changed the textural properties of the catalyst from non porous to porous. FESEM and TEM were used to study the morphology of the catalyst. It was determined that the addition of niobium to the catalyst changed the shape of the cobalt particles from spherical to hexagonal structure. Fringes seen on the particles indicate that they are in the form of crystals. TEM results also indicated that the particles were well dispersed on the support. Agglomeration of particles was seen in some images. This might to due to mistakes made during the catalyst synthesis. The catalytic activity of the silica supported cobalt and niobium bimetallic catalysts were evaluated in a fixed bed reactor at 220°C and 1 bar. The results obtained from the reactor were quite satisfactory. Maximum CO conversion obtained was 70.07% using sample D (85Co15Nb). The selectivity towards CH<sub>4</sub> was minimal. Most of the hydrocarbons formed were within C<sub>2</sub>-C<sub>4</sub> range. The synthesized catalysts samples displayed high olefin productivity compared to paraffin in the FTS indicating the catalysts are more suitable for olefin production.

## 6.2 RECOMMENDATIONS

Based on the observations made during this study, a few recommendations that can be drawn for future work in this area are as follows:

- Due to the fact that the physiochemical properties of the catalyst affect the overall performance of the catalyst in the FTS, improvements to the catalyst properties such as higher dispersion of metal particle can be made by varying the composition of the catalyst and synthesis technique.
- Since the agglomeration of the metal particles on the support are dependent on the amount and flow rate of emulsion destabilizing agent, it is important to find the correct amount and flow rate to be used.
- FTS is generally conducted at high pressure conditions. Therefore it is recommended that the reaction is done under high pressure preferably 15-20 bars.
- Different sets of reaction conditions should be tested to find the most optimum condition for the cobalt and niobium bimetallic catalysts.

## REFERENCES

1. Zhang, Q., W. Deng, and Y. Wang, *Recent advances in understanding the key catalyst factors for Fischer-Tropsch synthesis*. Journal of Energy Chemistry, 2013. **22**(1): p. 27-38.
2. Masters, C., *The Fischer-Tropsch reaction*. Advances in Organometallic Chemistry, 1979. **17**: p. 61-103.
3. Ali, S., N.A.M. Zabidi, and D. Subbarao, *Correlation between Fischer-Tropsch catalytic activity and composition of catalysts*. Chemistry Central Journal, 2011. **2011**(5): p. 68.
4. Bartholomew, C.H. and R.J. Farrauto, *Hydrogen production and synthesis gas reactions*. Fundamentals of Industrial Catalytic Processes, Second Edition, 2006: p. 339-486.
5. Dry, M.E., *The Fischer-Tropsch process: 1950-2000*. Catalysis today, 2002. **71**(3): p. 227-241.
6. Bartholomew, C.H. *History of cobalt catalyst design for FTS*. in *Proceedings of the National Spring Meeting of the American Institute of Chemical Engineers (AIChE'03)*. 2003.
7. Davis, B.H., *Fischer-Tropsch synthesis: relationship between iron catalyst composition and process variables*. Catalysis today, 2003. **84**(1): p. 83-98.
8. Steynberg, A. and M. Dry, *Fischer-Tropsch Technology*. 2004: Elsevier.
9. TASFY, S.F.H.T., *PERFORMANCE AND CHARACTERIZATION OF SUPPORTED IRON NANOCATALYST IN FISCHER-TROPSCH REACTION*. 2011, UNIVERSITI TEKNOLOGI PETRONAS.
10. Xu, J., *Rational Design of Silica-Supported Platinum Promoted Iron Fischer-Tropsch Synthesis Catalysts Based on Activity-Structure Relationships*. 2003, Brigham Young University. Department of Chemical Engineering.
11. Anderson, R., R. Friedel, and H. Storch, *Fischer-Tropsch Reaction Mechanism Involving Stepwise Growth of Carbon Chain*. The Journal of Chemical Physics, 1951. **19**(3): p. 313-319.

12. Hayakawa, H., H. Tanaka, and K. Fujimoto, *Studies on catalytic performance of precipitated iron/silica catalysts for Fischer–Tropsch Synthesis*. Applied Catalysis A: General, 2007. **328**(2): p. 117-123.
13. Shroff, M.D., et al., *Activation of precipitated iron Fischer-Tropsch synthesis catalysts*. Journal of Catalysis, 1995. **156**(2): p. 185-207.
14. Khodakov, A.Y., W. Chu, and P. Fongarland, *Advances in the development of novel cobalt Fischer-Tropsch catalysts for synthesis of long-chain hydrocarbons and clean fuels*. Chemical Reviews, 2007. **107**(5): p. 1692-1744.
15. Li, T., et al., *Study on an iron–nickel bimetallic Fischer–Tropsch synthesis catalyst*. Fuel Processing Technology, 2014. **118**: p. 117-124.
16. Vannice, M., *The catalytic synthesis of hydrocarbons from H<sub>2</sub>CO mixtures over the group VIII metals: I. The specific activities and product distributions of supported metals*. Journal of Catalysis, 1975. **37**(3): p. 449-461.
17. Diehl, F. and A.Y. Khodakov, *Promotion of cobalt Fischer-Tropsch catalysts with noble metals: a review*. Oil & Gas Science and Technology-Revue de l'IFP, 2009. **64**(1): p. 11-24.
18. Ali, S., N.A.M. Zabidi, and D. Subbarao, *Development of niobium-promoted cobalt catalysts on carbon nanotubes for Fischer-Tropsch synthesis*. Journal of Natural Gas Chemistry, 2011. **20**(6): p. 659-663.
19. Zabidi, N.M., *Synthesis of Nanocatalysts via Reverse Microemulsion Route for Fischer-Tropsch Reactions*.
20. Eriksson, S., et al., *Preparation of catalysts from microemulsions and their applications in heterogeneous catalysis*. Applied Catalysis A: General, 2004. **265**(2): p. 207-219.
21. Zielińska-Jurek, A., et al., *Nanoparticles preparation using microemulsion systems*. 2012.

## APPENDICES

### APPENDIX I. CALCULATION

#### AMOUNT OF SUPPORT AND METAL FOR CATALYST PREPARATION

Sample size: 3.0 gram catalyst

Mass of catalyst = mass of metal + mass of support

Percentage (%) of metal loading: 5 wt% metal of the catalyst

$$\text{Mass of metal} = \left( \frac{5}{100} \times 3.0 \text{ g catalyst} \right) = 0.15 \text{ g metal}$$

Mass of support = Mass of catalyst – Mass of metal

$$= 3.0 \text{ g catalyst} - 0.15 \text{ g metal}$$

$$= 2.85 \text{ g of support}$$

#### AMOUNT OF COBALT NITRATE AND AMMONIUM NIOBIUM OXALATE FOR CATALYST PERPARTION

Table I.1 shows the different compositions of Cobalt and Niobium used for the preparation of the catalyst.

**Table I.1.** Metal Composition

Sample	Composition of Co:Nb (5 wt%)
A	100:00:00
B	95:05:00
C	90:10:00
D	85:15:00
E	80:20:00

Mass of metal = 0.15 g

Molecular weight of Cobalt Nitrate  $\text{Co}(\text{NO}_3)_2 \cdot 6\text{H}_2\text{O}$ : 291.04 g/mol

Molecular weight of Ammonium Niobium Oxalate  $\text{C}_4\text{H}_4\text{NNbO}_9 \cdot 6\text{H}_2\text{O}$ : 302.98 g/mol

**A) Co:Nb; 100:0**

For (Co:Nb at 100:0), 100% of metal loading is cobalt, thus the mass of cobalt metal needed is 0.15 g which comes in the form of  $\text{Co}(\text{NO}_3)_2 \cdot 6\text{H}_2\text{O}$ .

Molecular weight of Co = 58.9 g/mol

$$\frac{0.15 \text{ g Co}}{58.9 \frac{\text{g}}{\text{mol}} \text{ Co}} \times 291.04 \frac{\text{g}}{\text{mol}} \text{ Co}(\text{NO}_3)_2 \cdot 6\text{H}_2\text{O} = 0.741 \text{ g Co}(\text{NO}_3)_2 \cdot 6\text{H}_2\text{O}$$

Therefore, in 0.741 g of  $\text{Co}(\text{NO}_3)_2 \cdot 6\text{H}_2\text{O}$  there is 0.15 g Co which is 5 wt% of the catalyst.

Hence the amount of  $\text{Co}(\text{NO}_3)_2 \cdot 6\text{H}_2\text{O}$  needed = 0.741 g.

**B) Co:Nb; 95:5**

$$\begin{aligned} \text{Mass of metal} &= 0.15 \text{ g of metal (5 wt\%)} = \left(0.15 \times \frac{95}{100}\right) + \left(0.15 \times \frac{5}{100}\right) \\ &= 0.143 \text{ g Co} + 0.007 \text{ g Nb} \end{aligned}$$

For Cobalt,

$$\frac{0.143 \text{ g Co}}{58.9 \frac{\text{g}}{\text{mol}} \text{ Co}} \times 291.04 \frac{\text{g}}{\text{mol}} \text{ Co}(\text{NO}_3)_2 \cdot 6\text{H}_2\text{O} = 0.707 \text{ g Co}(\text{NO}_3)_2 \cdot 6\text{H}_2\text{O}$$

For Niobium,

Molecular weight of Co = 92.9 g/mol

$$\frac{0.007 \text{ g Nb}}{92.9 \frac{\text{g}}{\text{mol}} \text{ Nb}} \times 302.98 \frac{\text{g}}{\text{mol}} \text{ C}_4\text{H}_4\text{NNbO}_9 \cdot 6\text{H}_2\text{O} = 0.023 \text{ g C}_4\text{H}_4\text{NNbO}_9 \cdot 6\text{H}_2\text{O}$$

**C) Co:Nb; 90:10**

$$\begin{aligned} \text{Mass of metal} &= 0.15 \text{ g of metal (5 wt\%)} = \left(0.15 \times \frac{90}{100}\right) + \left(0.15 \times \frac{10}{100}\right) \\ &= 0.135 \text{ g Co} + 0.015 \text{ g Nb} \end{aligned}$$

For Cobalt,

$$\frac{0.135 \text{ g Co}}{58.9 \frac{\text{g}}{\text{mol}} \text{ Co}} \times 291.04 \frac{\text{g}}{\text{mol}} \text{ Co(NO}_3)_2 \cdot 6\text{H}_2\text{O} = 0.667 \text{ g Co(NO}_3)_2 \cdot 6\text{H}_2\text{O}$$

For Niobium,

$$\frac{0.015 \text{ g Nb}}{92.9 \frac{\text{g}}{\text{mol}} \text{ Nb}} \times 302.98 \frac{\text{g}}{\text{mol}} \text{ C}_4\text{H}_4\text{NNbO}_9 \cdot 6\text{H}_2\text{O} = 0.049 \text{ g C}_4\text{H}_4\text{NNbO}_9 \cdot 6\text{H}_2\text{O}$$

**D) Co:Nb; 85:15**

$$\begin{aligned} \text{Mass of metal} &= 0.15 \text{ g of metal (5 wt\%)} = \left(0.15 \times \frac{85}{100}\right) + \left(0.15 \times \frac{15}{100}\right) \\ &= 0.128 \text{ g Co} + 0.022 \text{ g Nb} \end{aligned}$$

For Cobalt,

$$\frac{0.128 \text{ g Co}}{58.9 \frac{\text{g}}{\text{mol}} \text{ Co}} \times 291.04 \frac{\text{g}}{\text{mol}} \text{ Co(NO}_3)_2 \cdot 6\text{H}_2\text{O} = 0.632 \text{ g Co(NO}_3)_2 \cdot 6\text{H}_2\text{O}$$

For Niobium,

$$\frac{0.022 \text{ g Nb}}{92.9 \frac{\text{g}}{\text{mol}} \text{ Nb}} \times 302.98 \frac{\text{g}}{\text{mol}} \text{ C}_4\text{H}_4\text{NNbO}_9 \cdot 6\text{H}_2\text{O} = 0.072 \text{ g C}_4\text{H}_4\text{NNbO}_9 \cdot 6\text{H}_2\text{O}$$

**E) Co:Nb; 80:20**

$$\begin{aligned} \text{Mass of metal} &= 0.15 \text{ g of metal (5 wt\%)} = \left(0.15 \times \frac{80}{100}\right) + \left(0.15 \times \frac{20}{100}\right) \\ &= 0.120 \text{ g Co} + 0.030 \text{ g Nb} \end{aligned}$$

For Cobalt,

$$\frac{0.120 \text{ g Co}}{58.9 \frac{\text{g}}{\text{mol}} \text{ Co}} \times 291.04 \frac{\text{g}}{\text{mol}} \text{ Co(NO}_3)_2 \cdot 6\text{H}_2\text{O} = 0.593 \text{ g Co(NO}_3)_2 \cdot 6\text{H}_2\text{O}$$

For Niobium,

$$\frac{0.030 \text{ g Nb}}{92.9 \frac{\text{g}}{\text{mol}} \text{ Nb}} \times 302.98 \frac{\text{g}}{\text{mol}} \text{ C}_4\text{H}_4\text{NNbO}_9 \cdot 6\text{H}_2\text{O} = 0.098 \text{ g C}_4\text{H}_4\text{NNbO}_9 \cdot 6\text{H}_2\text{O}$$

**Table I.2.** Appropriate amount of metal

Samples					
No.	A	B	C	D	E
Composition	Co:Nb (100:0)	Co:Nb (95:5)	Co:Nb (90:10)	Co:Nb (85:15)	Co:Nb (80:20)
Amount of $\text{Co}(\text{NO}_3)_2 \cdot 6\text{H}_2\text{O}$ (g)	0.741	0.707	0.667	0.632	0.593
Amount of $\text{C}_4\text{H}_4\text{NNbO}_9 \cdot 6\text{H}_2\text{O}$ (g)	0.000	0.023	0.049	0.072	0.098
Net Total	0.741	0.730	0.716	0.704	0.691

### AMOUNT OF WATER TO SURFACTANT

Based on previous research work, the suitable molarity of Triton X-114 in the Cyclohexane is 0.2 M and the optimum molar ratio of water to surfactant is 3:1

Molarity of Triton X-114 = 0.2 M

Mol of Triton = Molarity (M) x Volume (L)

$$= 0.2 \text{ M} \times 0.1 \text{ L}$$

$$= 0.02 \text{ mol}$$

The ratio of 3:1 (water-to-surfactant) is best suited for 0.02 mol of Triton X-114 in Cyclohexane which forms a homogenous solution at this critical micelle concentration. The calculation to determine the mass of Triton X-114 and water needed are as follows”

$\text{H}_2\text{O}$  : Triton X-114

3 : 1

0.06 : 0.02

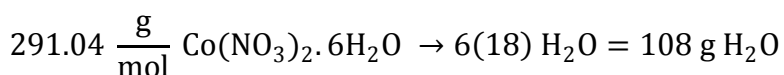
Mass of Triton X-114 = 0.02 mol x 558.75 g/mol Triton X-114

$$= 11.175 \text{ g Triton X-114}$$

$$n\text{H}_2\text{O} = \frac{\text{Mass of H}_2\text{O}}{\text{MW of H}_2\text{O}}$$

$$\begin{aligned} \text{Mass of H}_2\text{O} &= n\text{H}_2\text{O} \times \text{MW H}_2\text{O} \\ &= 0.06 \text{ mol} \times 18 \text{ g/mol} \\ &= 1.080 \text{ g H}_2\text{O} \end{aligned}$$

**A) Co:Nb; 100:0**

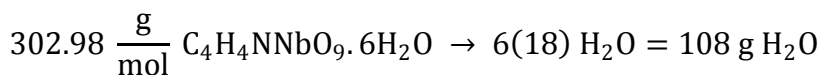


$$\frac{108 \text{ g H}_2\text{O}}{291.04 \text{ g Co}(\text{NO}_3)_2 \cdot 6\text{H}_2\text{O}} = 0.371 \text{ g H}_2\text{O in 1 g Co}(\text{NO}_3)_2 \cdot 6\text{H}_2\text{O}$$

Therefore for 0.741 g  $\text{Co}(\text{NO}_3)_2 \cdot 6\text{H}_2\text{O} \rightarrow 0.275 \text{ g H}_2\text{O}$  (Mass of water in metal precursor)

$$\begin{aligned} \text{Mass of H}_2\text{O required} &= 1.080 \text{ g} - 0.275 \text{ g} \\ &= 0.805 \text{ g H}_2\text{O} \end{aligned}$$

**B) Co:Nb; 95:5**



$$\frac{108 \text{ g H}_2\text{O}}{302.98 \text{ g C}_4\text{H}_4\text{NNbO}_9 \cdot 6\text{H}_2\text{O}} = 0.356 \text{ g H}_2\text{O in 1 g C}_4\text{H}_4\text{NNbO}_9 \cdot 6\text{H}_2\text{O}$$

Therefore for 0.023 g  $\text{C}_4\text{H}_4\text{NNbO}_9 \cdot 6\text{H}_2\text{O} \rightarrow 0.008 \text{ g H}_2\text{O}$  (Mass of water in metal precursor)

And

For 0.707 g  $\text{Co}(\text{NO}_3)_2 \cdot 6\text{H}_2\text{O} \rightarrow 0.262 \text{ g H}_2\text{O}$  (Mass of water in metal precursor)

$$\begin{aligned} \text{Mass of H}_2\text{O required} &= 1.080 \text{ g} - 0.008 - 0.262 \text{ g} \\ &= 0.810 \text{ g H}_2\text{O} \end{aligned}$$

**C) Co:Nb; 90:10**

0.049 g  $\text{C}_4\text{H}_4\text{NNbO}_9 \cdot 6\text{H}_2\text{O} \rightarrow 0.017 \text{ g H}_2\text{O}$  (Mass of water in metal precursor)

0.667 g  $\text{Co}(\text{NO}_3)_2 \cdot 6\text{H}_2\text{O}$   $\rightarrow$  0.247 g  $\text{H}_2\text{O}$  (Mass of water in metal precursor)

Mass of  $\text{H}_2\text{O}$  required = 1.080 g – 0.017 – 0.247 g

$$= 0.816 \text{ g } \text{H}_2\text{O}$$

**D) Co:Nb; 85:15**

0.072 g  $\text{C}_4\text{H}_4\text{NNbO}_9 \cdot 6\text{H}_2\text{O}$   $\rightarrow$  0.025 g  $\text{H}_2\text{O}$  (Mass of water in metal precursor)

0.632 g  $\text{Co}(\text{NO}_3)_2 \cdot 6\text{H}_2\text{O}$   $\rightarrow$  0.234 g  $\text{H}_2\text{O}$  (Mass of water in metal precursor)

Mass of  $\text{H}_2\text{O}$  required = 1.080 g – 0.025 – 0.234 g

$$= 0.821 \text{ g } \text{H}_2\text{O}$$

**E) Co:Nb; 80:20**

0.098 g  $\text{C}_4\text{H}_4\text{NNbO}_9 \cdot 6\text{H}_2\text{O}$   $\rightarrow$  0.035 g  $\text{H}_2\text{O}$  (Mass of water in metal precursor)

0.593 g  $\text{Co}(\text{NO}_3)_2 \cdot 6\text{H}_2\text{O}$   $\rightarrow$  0.220 g  $\text{H}_2\text{O}$  (Mass of water in metal precursor)

Mass of  $\text{H}_2\text{O}$  required = 1.080 g – 0.035 – 0.220 g

$$= 0.825 \text{ g } \text{H}_2\text{O}$$

**Table I.3** Amount of water to surfactant

Samples					
No.	A	B	C	D	E
Molar Ratio	3:1	3:1	3:1	3:1	3:1
Mass Triton X-114 (g)	11.175	11.175	11.175	11.175	11.175
Mass of Water (g)	1.080	1.080	1.080	1.080	1.080
Mass of Water in Metal precursor (g)	0.275	0.270	0.264	0.259	0.255
Mass of Water required (g)	0.805	0.810	0.816	0.821	0.825

**AMOUNT OF HYDRAZINE**

Another chemical which is added to each sample is Hydrazine ( $\text{N}_2\text{H}_2$ ). Hydrazine is added to each sample solution to improve metal nanoparticles formation in the core of water micelles by reducing cobalt oxide and niobium oxide. Hydrazine is added at

a ratio of 10:1 (hydrazine – Co/Nb) in each sample and the calculations are as follows:

n Hydrazine : n Metal ( total for both Co and Nb)

10 : 1

**A) Co:Nb; 100:0**

Mass of Co = 0.15 g

$$n = \frac{\text{Mass of Co}}{\text{MW of Co}} = \frac{0.15 \text{ g Co}}{58.9 \frac{\text{g}}{\text{mol}} \text{ Co}} = 0.00254 \text{ mol Co}$$

Therefore, mole ratio of hydrazine to pure cobalt is 0.0254:0.00254

$$\begin{aligned} \text{Mass of Hydrazine} &= 0.0254 \times 32.05 \text{ g/mol hydrazine} \\ &= 0.814 \text{ g hydrazine} \end{aligned}$$

**B) Co:Nb; 95:5**

Mass of Co = 0.143

$$n = \frac{\text{Mass of Co}}{\text{MW of Co}} = \frac{0.143 \text{ g Co}}{58.9 \frac{\text{g}}{\text{mol}} \text{ Co}} = 0.0024 \text{ mol Co}$$

Mass of Nb = 0.007

$$n = \frac{\text{Mass of Nb}}{\text{MW of Nb}} = \frac{0.007 \text{ g Nb}}{92.9 \frac{\text{g}}{\text{mol}} \text{ Nb}} = 0.000075 \text{ mol Nb}$$

Total number of mol = 0.0024 + 0.000075 = 0.002475

Therefore, mole ratio of hydrazine to pure cobalt is 0.02475:0.002475

$$\begin{aligned} \text{Mass of Hydrazine} &= 0.02475 \times 32.05 \text{ g/mol hydrazine} \\ &= 0.793 \text{ g hydrazine} \end{aligned}$$

**C) Co:Nb; 90:10**

Mass of Co = 0.135 g Co

$$n = \frac{\text{Mass of Co}}{\text{MW of Co}} = \frac{0.135 \text{ g Co}}{58.9 \frac{\text{g}}{\text{mol}} \text{ Co}} = 0.0023 \text{ mol Co}$$

Mass of Nb = 0.015 g

$$n = \frac{\text{Mass of Nb}}{\text{MW of Nb}} = \frac{0.015 \text{ g Nb}}{92.9 \frac{\text{g}}{\text{mol}} \text{ Nb}} = 0.00016 \text{ mol Nb}$$

Total number of mol = 0.0023 + 0.00016 = 0.00246

Therefore, mole ratio of hydrazine to pure cobalt is 0.0246:0.00246

$$\begin{aligned} \text{Mass of Hydrazine} &= 0.0246 \times 32.05 \text{ g/mol hydrazine} \\ &= 0.788 \text{ g hydrazine} \end{aligned}$$

#### **D) Co:Nb; 85:15**

Mass of Co = 0.128 g

$$n = \frac{\text{Mass of Co}}{\text{MW of Co}} = \frac{0.128 \text{ g Co}}{58.9 \frac{\text{g}}{\text{mol}} \text{ Co}} = 0.0022 \text{ mol Co}$$

Mass of Nb = 0.022 g

$$n = \frac{\text{Mass of Nb}}{\text{MW of Nb}} = \frac{0.022 \text{ g Nb}}{92.9 \frac{\text{g}}{\text{mol}} \text{ Nb}} = 0.00024 \text{ mol Nb}$$

Total number of mol = 0.0022 + 0.00024 = 0.00244

Therefore, mole ratio of hydrazine to pure cobalt is 0.0244:0.00244

$$\begin{aligned} \text{Mass of Hydrazine} &= 0.0244 \times 32.05 \text{ g/mol hydrazine} \\ &= 0.782 \text{ g hydrazine} \end{aligned}$$

#### **E) Co:Nb; 80:20**

Mass of Co = 0.120 g

$$n = \frac{\text{Mass of Co}}{\text{MW of Co}} = \frac{0.120 \text{ g Co}}{58.9 \frac{\text{g}}{\text{mol}} \text{ Co}} = 0.00204 \text{ mol Co}$$

Mass of Nb = 0.030 g

$$n = \frac{\text{Mass of Nb}}{\text{MW of Nb}} = \frac{0.030 \text{ g Nb}}{92.9 \frac{\text{g}}{\text{mol}} \text{ Nb}} = 0.000323 \text{ mol Nb}$$

Total number of mol = 0.00204 + 0.000323 = 0.002363

Therefore, mole ratio of hydrazine to pure cobalt is 0.02363:0.002363

Mass of Hydrazine = 0.02363 X 32.05 g/mol hydrazine

$$= 0.757 \text{ g hydrazine}$$

**Table I.4.** Amount of Hydrazine

Samples					
No.	A	B	C	D	E
Total mole of Co and Nb	0.00254	0.002475	0.00246	0.00244	0.002363
Molar ratio	10:1	10:1	10:1	10:1	10:1
Amount of hydrazine	0.814	0.793	0.788	0.782	0.757

## APPENDIX II. RAW DATA FOR BET

Pore Diameter (Å)	dA/dlog(D) Pore Area (m <sup>2</sup> /g·Å)
2807.494	0.04429
2166.308	0.061095
1734.19	0.095784
1435.911	0.120528
1203.118	0.156041
1046.325	0.22225
861.0238	0.206659
707.6524	0.321605
607.0585	0.383158
531.0476	0.438058
468.91	0.551695
417.873	0.671379
358.2177	0.689763
305.7572	0.789976
266.9595	0.831321
236.6043	0.873509
212.043	0.868582
190.9687	0.851034
157.9055	0.835295
123.7079	0.811668
99.85195	0.726373
83.32333	0.760494
71.25847	0.850345
62.03447	0.687032
54.68671	0.915663
48.72261	0.856959
43.74526	0.833651
39.50749	1.055642
35.84982	0.747855
32.6385	1.132088
29.78222	1.544045
27.2373	1.939778
25.5437	2.098315
24.40734	2.053026
23.17565	2.922261
21.87653	3.015134
20.62658	3.601423
19.41617	3.718476
18.22895	4.896159
17.05908	4.489509

**Table II.1:** BJH Adsorption dA/dlog(D) Pore Area data for sample A

Isotherm Linear Plot of 100Co/SiO <sub>2</sub>	
Relative Pressure (p/p°)	Quantity Adsorbed (cm <sup>3</sup> /g STP)
0.013344295	0.362053591
0.032081361	0.428423305
0.064541917	0.493916289
0.074840725	0.511656479
0.089894728	0.534175952
0.109818733	0.564335734
0.134902574	0.596712124
0.150081038	0.616102345
0.174901605	0.643882449
0.199868343	0.672384361
0.224783375	0.696679741
0.249617412	0.72046435
0.274680656	0.742497387
0.299554232	0.764337805
0.319689012	0.779422937
0.339838431	0.794994983
0.379030211	0.825173773
0.418972457	0.854406237
0.458922504	0.881677871
0.498809365	0.906680974
0.538687451	0.938608966
0.578697958	0.97073451
0.618370972	1.007576222
0.658459387	1.052616906
0.698360458	1.098425055
0.738063994	1.162129905
0.778244576	1.239496736
0.817878674	1.34022769
0.857658426	1.501898058
0.888226578	1.702378266
0.899399181	1.808335909
0.909696941	1.930419211
0.91965152	2.07782292
0.929615618	2.257341098
0.939294368	2.475898558
0.949541073	2.757078389
0.954946196	2.953247052
0.960199252	3.152835426
0.96510515	3.345096736
0.969785372	3.556777189

**Table II.2:** Isotherm Linear Plot data for sample A

### APPENDIX III. MAPPING FROM EDX

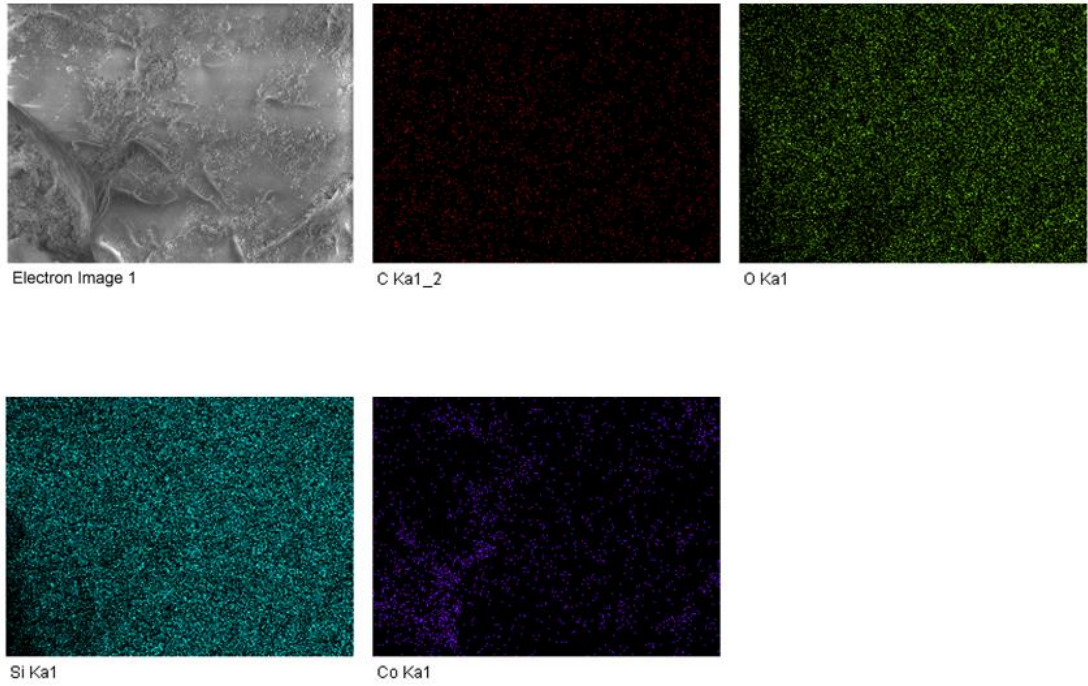


Figure III.1: Mapping for sample A

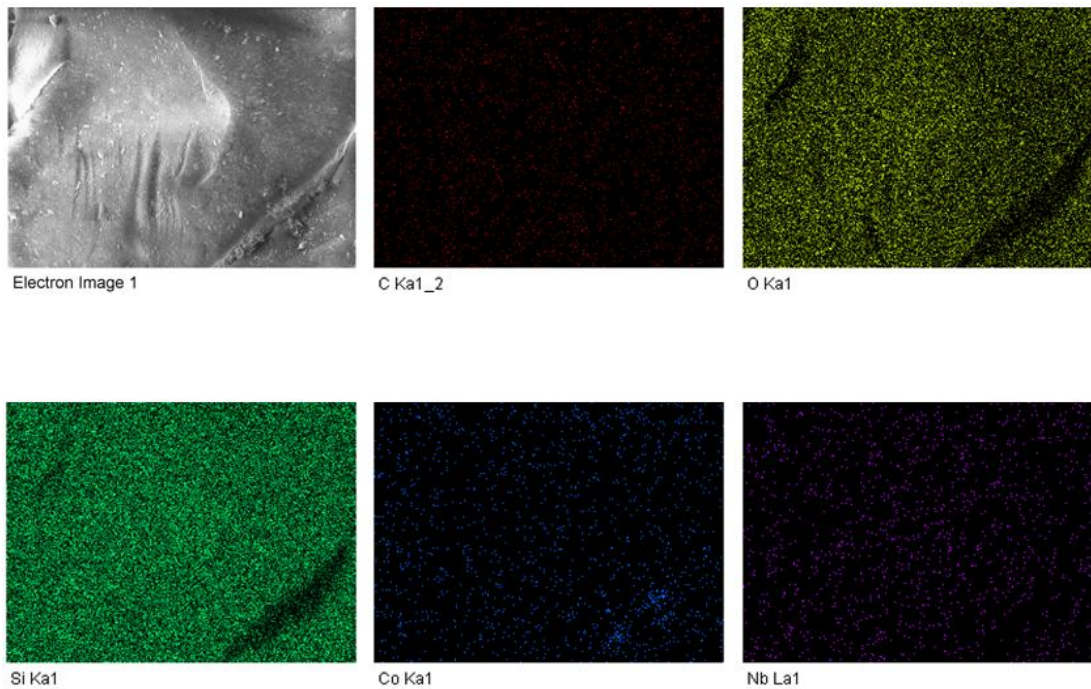
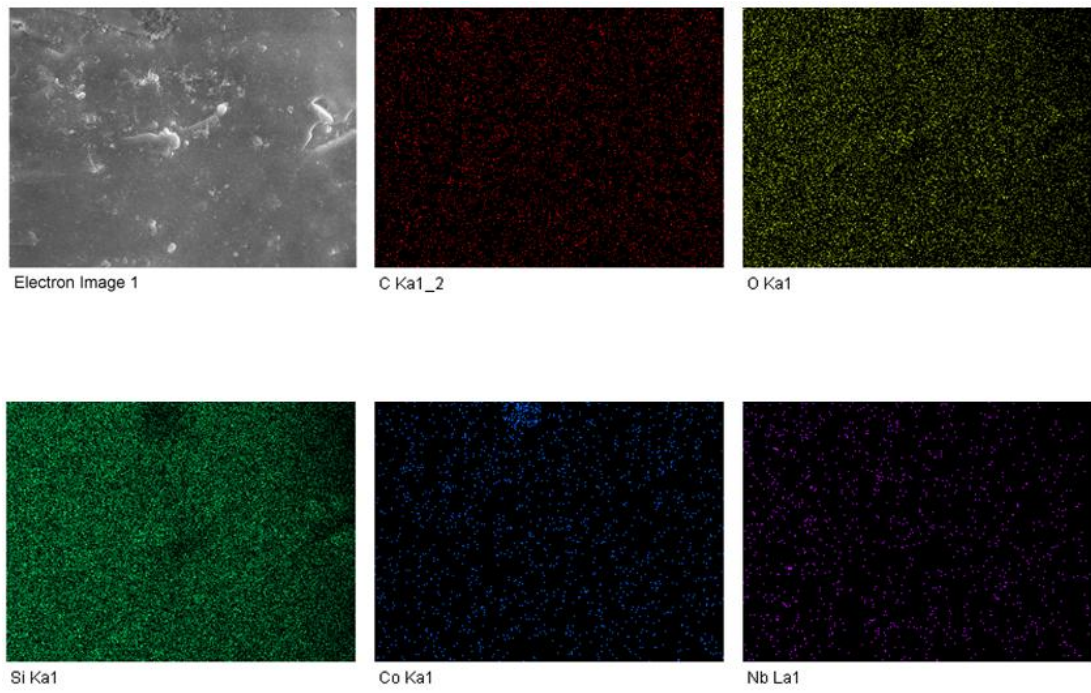
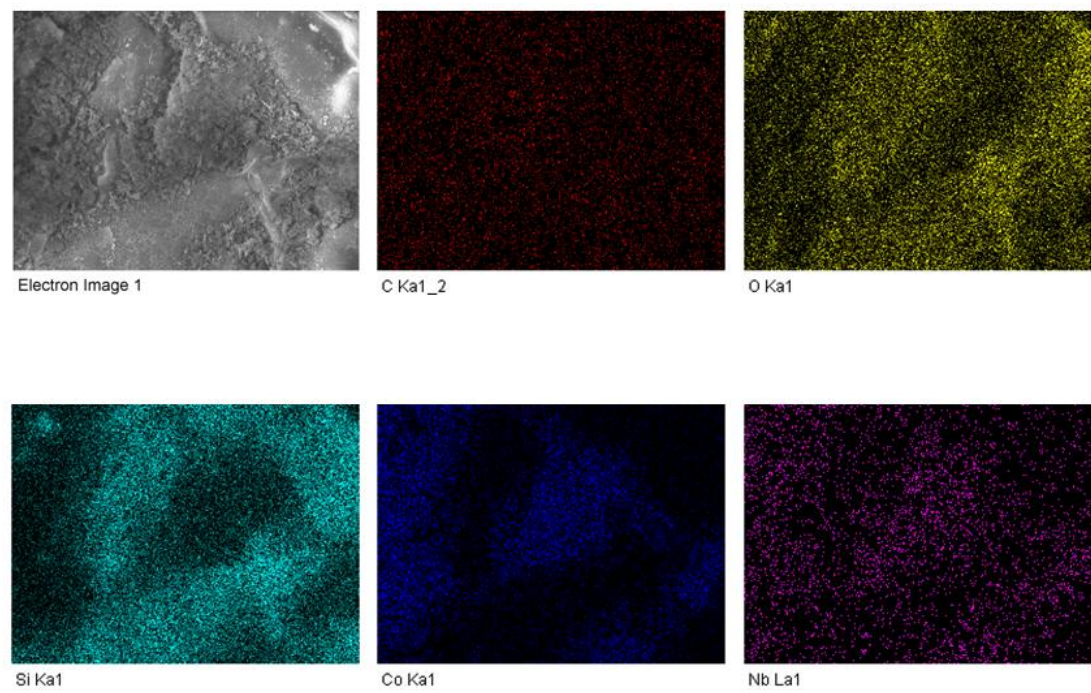


Figure III.2: Mapping for sample B



**Figure III.3:** Mapping for sample C



**Figure III.3:** Mapping for sample D